Future Foods 13 (2026) 101032

Contents lists available at ScienceDirect

Future Foods

journal homepage: www.elsevier.com/locate/fufo

Machine learning-guided optimization of probiotic chickpea milk fermentation enhances antioxidant capacity, volatile aroma profile, and sensory quality

Ping Tang [a], Siew-Young Quek [b,1], Yi-Chen Lo [c], Somayeh Gholivand [a], Ming-Yang Cui [d], Aliah Zannierah Mohsin [a], Nurul Hanisah Juhari [a], Anis Shobirin Meor Hussin [a,*]

[a] Faculty of Food Science and Technology, Universiti Putra Malaysia, 43400 UPM Serdang, Selangor Darul Ehsan, Malaysia
[b] Food Science, School of Chemical Sciences, Faculty of Science, University of Auckland, Auckland 1010, New Zealand
[c] Institute of Food Science and Technology, National Taiwan University, Taipei, 10617, Taiwan
[d] Department of Food Nutrition and Health, School of Food Engineering, East University of Heilongjiang, 150066 Harbin, Heilongjiang, China

ARTICLE INFO

Keywords:
Fermentation
Optimization
Lactic acid bacteria
Artificial neural network
Machine learning

ABSTRACT

This study developed and optimized a probiotic chickpea milk fermentation process using *Lactiplantibacillus plantarum* PC4, integrating response surface methodology with artificial neural network genetic algorithm (ANN—NSGA-II) modeling. Fermentation parameters (time, temperature, inoculum level) were systematically evaluated for their effects on antioxidant activity (DPPH, FRAP, TPC), pH, and probiotic viability. Although response surface models showed strong fitting accuracy ($R^2 > 0.96$), ANN demonstrated superior prediction stability and captured nonlinear behavior across all responses (Test $R^2 > 0.97$). Multi-objective optimization using NSGA-II maximized antioxidant capacity and viable cell counts while maintaining pH near 4.5. The optimal compromise solution (7.40 h, 35.95 °C, 2.22 %) achieved high antioxidant values and 8.81 log CFU/mL viable probiotics, with validation experiments demonstrated reasonable agreement between the predicted and experimental results. Fermentation enhanced β-glucosidase activity, lactic acid accumulation, and the formation of alcohols and esters, while markedly reducing aldehyde-driven beany odor. Sensory evaluation confirmed stronger fermented aroma, lower beany notes, and improved overall flavor. These findings establish ANN—NSGA-II as an effective and precise framework for developing functional plant-based fermented beverages.

1. Introduction

Chickpea (*Cicer arietinum* L.) is a widely cultivated legume valued for its high protein, complex carbohydrates, dietary fiber, minerals, and bioactive compounds such as polyphenols and saponins (Lopes et al., 2020; Rincon et al., 2020). Compared with other legumes, chickpea has lower fat content and minimal allergenicity, which makes it attractive for developing allergen free, protein enriched plant-based milk alternatives (Vallath and Shanmugam, 2022). Driven by lactose intolerance, milk protein allergies, vegan diets, and environmental concerns, demand for dairy alternatives has increased. Many cereal and nut-based beverages are already commercialized but often show low protein density and nutritional imbalance (Lopes et al., 2020). In contrast, chickpea-based milk offers higher protein content, favorable emulsifying properties, and a relatively low glycemic index, although its use is still limited by beany flavor, poor protein solubility, and residual antinutritional factors such as phytic acid and oligosaccharides (Abadl et al., 2023; Pennells et al., 2024; Wang et al., 2018).

A range of processing strategies, including heat treatment, enzymatic modification, ultrasonication, and especially fermentation, has been applied to improve the sensory quality, digestibility, and nutrient bioavailability of legume-based beverages. Chickpea milk is a promising substrate for probiotic delivery because its macronutrient profile supports microbial growth while allowing the development of value-added

* Corresponding author.
E-mail address: shobirin@upm.edu.my (A.S. Meor Hussin).
[1] Given their role as Co-Editor-in-Chief, Siew-Young Quek had no involvement in the peer review of this article and had no access to information regarding its peer review. Full responsibility for the editorial process for this article was delegated to another journal editor.

https://doi.org/10.1016/j.fufo.2026.101032
Received 3 March 2026; Received in revised form 12 April 2026; Accepted 6 May 2026
Available online 7 May 2026

functional drinks with improved antioxidant properties and viable cell counts. Lactic acid bacteria (LAB) are widely employed in plant-based fermentations due to their metabolic versatility and resilience in non-dairy matrices (Abbaspour, 2024; Chaturvedi and Chakraborty, 2021). LAB can hydrolyze complex macromolecules and release phenolic and flavonoid compounds, thereby enhancing antioxidant capacity, while producing organic acids, exopolysaccharides, and short chain metabolites that improve palatability, texture, and potential health benefits (De Villa et al., 2023; Jayasree Joshi et al., 2024).

The performance of *Lactiplantibacillus plantarum* in chickpea milk is strongly influenced by fermentation variables such as temperature, incubation time, inoculum level, and initial pH. These factors act in a nonlinear and sometimes antagonistic manner on microbial growth, acidification, and the synthesis of bioactive metabolites (Mishra et al., 2014). Response surface methodology (RSM) remains a common tool for studying such systems, since it can identify significant factors and second order interactions (Pavani et al., 2024). However, RSM assumes quadratic relationships and can be inadequate for highly nonlinear or strongly coupled bioprocesses (Zhang et al., 2023). One factor at a time designs and simple linear models are even less suitable for capturing the complex dynamics of plant-based fermentations, and they often fail to provide reliable guidance for multi response optimization (Okoro et al., 2025). Artificial neural networks (ANN) have therefore gained attention as flexible data driven models that can approximate complex input output relationships in food processes (Bhagya Raj and Dash, 2022).

Although ANN models show strong predictive ability, they do not inherently supply optimal operating conditions and must be combined with external optimization algorithms (Wang and Kang, 2022). Chickpea milk fermentation presents a multi-response optimization challenge because nonlinear interactions among microbial growth, antioxidant formation, and acidification drive several quality attributes simultaneously. These interdependent responses can follow competing trends (e.g., maximizing antioxidant capacity while controlling pH and maintaining viable LAB), making single-objective optimization insufficient for achieving balanced product quality. The non-dominated sorting genetic algorithm II (NSGA-II) is a widely used multi-objective evolutionary algorithm that can generate Pareto optimal solutions for multiple, often conflicting, quality targets (Nametala et al., 2020; Verma et al., 2021; Zăvoianu et al., 2013). Hybrid ANN—NSGA-II frameworks thus allow simultaneous prediction and global optimization in complex food systems with several responses (Yu et al., 2016). In a fermentation case study, an EKF-ANN coupled with NSGA-II generated Pareto-optimal solutions and improved the target bioactives by 13.34 % (flavonoids) and 7.92 % (two benzoquinones) at the selected compromise point (Zheng et al., 2016). Despite the rapid growth of plant based fermented beverages, there is still limited work on chickpea milk that integrates ANN based modeling with multi-objective optimization. This study therefore aimed to (i) quantify the effects of key fermentation variables on antioxidant activity, pH, and probiotic viability in chickpea milk, (ii) develop predictive models using RSM and ANN, (iii) apply NSGA-II to the ANN model to identify optimal fermentation conditions, and (iv) compare the predictive performance and optimization efficiency of the RSM and ANN—NSGA-II approaches.

2. Materials and methods

2.1. Raw material and starter culture

Chickpeas (*Cicer arietinum* L.) were purchased from AEON supermarket in Selangor, Malaysia, and stored at room temperature until used. *Lactiplantibacillus plantarum* PC4, originally isolated from carrot pickle, was selected as the starter culture in this study. The strain was obtained from the Faculty of Food Science and Technology, Universiti Putra Malaysia.

2.2. Preparation of chickpea milk and starter culture

Chickpea milk was prepared as previously described, with minor modifications (Ping et al., 2025). Briefly, chickpeas were soaked overnight to achieve sufficient hydration, followed by wet grinding with distilled water at a 1:8 (w/v) ratio. The resulting slurry was filtered through sterile gauze to eliminate coarse particulates. The filtrate was then refrigerated at 4 °C overnight to facilitate starch sedimentation. Subsequently, sucrose was incorporated at a final concentration of 6 % (w/v), and the mixtures were subjected to heat treatment in a water bath at 90 °C for 15 minutes. After thermal processing, the samples were allowed to cool to room temperature before inoculation. Lactic acid bacterial strains were cultured in 10 mL of De Man, Rogosa, and Sharpe (MRS) broth (Oxoid, Hampshire, UK) at 37 °C for 24 h. Subsequently, the cultures were centrifugated at 3500 rpm (approximately 1370 × *g*, *r* = 10.0 cm) for 3 min (Sigma Sartorius 3–18 K, Göttingen, Germany) to pellet the cells. The harvested biomass was then rinsed three times with sterile 0.8 % (w/v) saline solution to remove residual media components.

2.3. Determination of microbial content of fermented chickpea milk

The proliferation of LAB strains in different substrate formulations was monitored via colony enumeration using the standard pour plate method. Serial 10-fold dilutions were prepared from 1 mL of sample, and 1 mL aliquots of each dilution were transferred into sterile Petri dishes. Subsequently, 15–20 mL of MRS agar (cooled to around 40 °C) was added, and the plates were rotated to ensure uniform dispersion before solidification. After solidification, the plates were incubated at 37 °C for 48 h under anaerobic conditions. Viable counts were recorded from plates containing 30–300 colonies, and LAB populations were expressed as CFU/mL according to Eq. (1):

$$\text{Number of LAB } \left(\text{CFU mL}^{-1}\right) = \text{Colonies counted} \times \text{Dilution factor} \times \frac{1}{\text{aliquot}} \quad (1)$$

2.4. Determination of antioxidant activity

2.4.1. DPPH radical scavenging activity

The DPPH (2,2-diphenyl-1-picrylhydrazyl) radical scavenging capacity was evaluated following the method of Abadl et al. (2023), with minor modifications. 0.1 mM DPPH methanolic solution was prepared and adjusted to an initial absorbance of 0.80–0.81 at 517 nm. Each sample was vortexed, centrifuged at 3500 rpm (approximately 1370 × *g*, *r* = 10.0 cm) for 5 min, and filtered through a 0.45 μm nylon membrane. Then, 1.0 mL of the filtrate was mixed with 2.5 mL of DPPH solution and incubated in the dark at room temperature for 30 min. The control consisted of DPPH mixed with distilled water. Absorbance was measured at 517 nm using a UV–visible spectrophotometer (BIOMATE 3, Thermo Fisher Scientific, USA), with water as blank. Results were calculated using a calibration curve and expressed as L-ascorbic acid equivalents (μg/mL).

2.4.2. Determination of ferric-reducing antioxidant power (FRAP)

With slight modifications, the ferric reducing antioxidant power (FRAP) assay was conducted based on Benzie and Strain (1999) method. The working FRAP reagent was freshly prepared by combining 10 mM TPTZ (2,4,6-tri(2-pyridyl)-s-triazine) in HCl, 20 mM $FeCl_3 \cdot 6H_2O$, and 30 mM sodium acetate buffer (pH 3.6) in a 1:1:10 ratio. 100 μL aliquot of each sample was added to 3.0 mL of the reagent, vortexed thoroughly, and incubated at room temperature in the dark for 30 min. Absorbance was recorded at 593 nm using a UV–vis spectrophotometer. The control consisted of distilled water in place of the sample. Results were expressed as mM $FeSO_4$ equivalents (mM/L), calculated from a standard

calibration curve.

2.4.3. Determination of total phenolic content

Total phenolic content (TPC) was determined according to the method of Yang et al. (2007), with minor modifications. Briefly, 200 μL of each sample was combined with 1.0 mL of 1:10 diluted Folin–Ciocalteu reagent, followed by adding 0.8 mL of 7.5 % (w/v) sodium carbonate solution. The reaction mixture was incubated at room temperature in the dark for 90 min. Absorbance was then recorded at 765 nm using a UV-visible spectrophotometer. TPC values were calculated from a gallic acid standard curve and expressed as μg gallic acid equivalents (GAE)/mL.

2.5. Determination of β-glucosidase activity

β-Glucosidase activity was determined using *p*-nitrophenyl-β-D-glucopyranoside (*p*-NPG) as the substrate, following the method of Matsuura et al. (1995) with slight modifications. Briefly, 0.1 mL of the sample was mixed with 0.9 mL of *p*-NPG solution (1 mmol/L in 0.05 mol/L citrate buffer, pH 4.8), and the reaction mixture was incubated at 37 °C for 10 min. The reaction was terminated by adding 0.5 mL of 0.5 mol/L Na_2CO_3 solution, and the release of *p*-nitrophenol (PNP) was quantified by measuring the absorbance at 405 nm using a V-visible spectrophotometer (BIOMATE 3, Thermo Fisher Scientific, USA). A calibration curve was constructed using PNP. Enzyme activity was expressed as units per milliliter (U/mL), where one unit (1 U) was defined as the amount of enzyme releasing 1 μmol of PNP per minute under the assay conditions. All assays were performed in triplicate, and results were expressed as mean ± standard deviation.

2.6. Determination of organic acid using HPLC

Sample preparation followed the procedure reported by Zhang et al. (2022) with slight modifications. Briefly, plant-based milk samples were centrifuged, and the resulting supernatant was passed through a 0.45 μm nylon membrane to eliminate suspended solids. Organic acid quantification was carried out according to Anzian et al. (2024). A Waters HPLC system (Waters Corporation, USA) equipped with a W2690/5 pump and a W2487 UV detector was employed, and data were processed using Empower 3 software (Build 3471, Waters Corporation, USA). For each analysis, 15 μL of the filtrate was injected into a LiChroCART®-RP18 column (300 mm × 7.8 mm, 5 μm particle size) fitted with a matching guard column (Merck, Darmstadt, Germany). The column oven was maintained at 35 °C. The mobile phase consisted of 0.004 N sulfuric acid (pH 2.1), which was filtered (0.45 μm) and degassed in an ultrasonic bath for 15 min prior to use. Isocratic elution was performed at a flow rate of 0.5 mL/min, and UV detection enabled the identification and quantification of organic acids. The analysis targeted citric acid, L-malic acid, D-tartaric acid, succinic acid, and L-lactic acid. Standard compounds were purchased from Sigma-Aldrich (Merck, Darmstadt, Germany) with a certified purity above 99.5 %. Mixed standard solutions at concentrations of 200, 400, 600, 800, and 1000 ppm were prepared and filtered before injection. Calibration curves were obtained by plotting the peak area of each compound against its concentration. All curves exhibited excellent linearity with coefficients of determination ($R^2 \geq 0.999$), confirming the robustness of the method for accurate quantification. Method validation (linearity, LOD, LOQ, recovery, precision) was performed according to ICH guidelines, and detailed results are provided in Supplementary Table S2.

2.7. Evaluation of volatile compounds

Volatile compounds were analyzed using a triple quadrupole gas chromatograph-mass spectrometer (GCMS-TQ8050NX, Shimadzu Corporation, Kyoto, Japan), following the method described by Chen et al. (2023) with some modifications. The headspace vial was purged with high-purity nitrogen to ensure complete removal of atmospheric gases prior to analysis. The thermo RSH autosampler was utilized to inject 3 mL of the sample. At the same time, the extraction fiber was preconditioned at 250 °C for 30 min within the gas chromatography inlet to ensure thermal stability and performance. The bake oven was maintained at 80 °C, the sample was equilibrated in a water bath for 20 min, and volatile compounds were extracted via SPME for 20 min. The fiber was subsequently desorbed in the GC inlet for 5 min, with the process automated by the SPME module and data collection initiated by the instrument control system. Quantification of volatiles was performed using the internal standard method, with Heptan-3-one (2-methyl-) added prior to extraction to correct for instrumental variability and matrix effects. Gas chromatographic separation was carried out on a TG-5MS capillary column using high-purity helium (99.999 %) as the carrier gas. Ionization was achieved in electron impact (EI) mode at an electron energy of 70 eV, and mass spectra were recorded over a scan range of 33–450 amu. The column temperature program was initiated at 50 °C with a 5 min hold, subsequently increased to 200 °C at a rate of 5 °C/min and maintained for 2 min, and finally raised to 230 °C at 10 °C/min with a final hold time of 3 min. Identification of volatile compounds was carried out by matching the obtained mass spectra (MS) and calculated retention indices (RIs, based on n-alkanes C5–C32) with reference data from the National Institute of Standards and Technology (NIST) database.

2.8. Sensory evaluation

A sensory panel ($n = 14$, 7 males and 7 females, aged 22–45 years) was recruited and trained to evaluate the intensity of sensory attributes of chickpea milk using the generalized labeled magnitude scale (gLM). All participants confirmed that they were free from food allergies, particularly to legumes or dairy products, and voluntarily agreed to participate by providing informed consent. The gLM scale ranged from 0 = "no sensation" to 9 = "strongest imaginable sensation of any kind," with intermediate anchors (1 = barely detectable, 5 = moderate, 7 = strong). The evaluated attributes included color uniformity (degree of evenness), beany flavor intensity, fermented aroma intensity, acidity intensity, thickness/viscosity, smoothness, and aftertaste intensity. Before the formal evaluation, panelists underwent structured training in two sessions. In the first session, the definitions of all sensory attributes were explained to establish a common understanding among panelists. The use of the generalized labeled magnitude scale (gLM) was also introduced, and panelists were instructed on how to relate perceived intensity to the scale anchors. In the second session, food-based reference materials were provided for attribute calibration. Beany flavor was represented by raw soybean soaking water (1:5, w/v, 2 h at room temperature), with the filtrate used as the high-intensity reference and a 1:1 dilution as the low-intensity reference. Acidity was calibrated with citric acid solutions (0.05 % and 0.15 %, w/v). Thickness was represented by corn starch suspensions (0.5 % and 2 %, w/v); and smoothness was illustrated by whole milk as a smooth reference and diluted okara suspension as a chalky reference. Panelists were asked to taste or observe these references and practice assigning intensity scores using the gLM scale.

Each sample (30 mL) was coded with randomized three-digit numbers and served at 10 ± 2 °C in a quiet, well-lit room free from extraneous odors. To minimize carry-over effects, bottled mineral water was provided for palate cleansing between samples. Panelists independently recorded their scores, and no discussion was permitted during the evaluation. The study protocol was approved by the Ethics Committee of Universiti Putra Malaysia (Reference No.: JKEUPM-2025–284).

2.9. Modelling procedure of RSM-CCD

Response Surface Methodology (RSM) based on a Central Composite Design (CCD) was employed to optimize the fermentation conditions of

chickpea milk. Three independent variables were selected: fermentation time (X_1, 4–8 h), temperature (X_2, 34–40 °C), and inoculum level (X_3, 1–3 % v/v). These variables were chosen based on preliminary experiments and relevant literature. Five response variables were evaluated: DPPH radical scavenging activity (Y_1), total phenolic content (Y_2), ferric reducing antioxidant power (Y_3), pH (Y_4), and probiotic viability (Y_5, log CFU/mL), as detailed in Table 1. A second-order polynomial model was fitted to describe the relationship between the independent variables and each response as follows (2):

$$Y = \beta_0 + \sum_{i=1}^{3} \beta_i X_i + \sum_{i=1}^{3} \beta_{ii} X_i^2 + \sum_{1 \le i < j \le 3} \beta_{ij} X_i X_j \quad (2)$$

where Y represents the predicted response, β_o is the intercept, β_i, β_{ii}, and β_{ij} denote the linear, quadratic, and interaction coefficients, respectively; and X_i and X_j represent the coded values of the independent variables, including fermentation time, temperature, and inoculum level.

2.10. Modelling procedure

2.10.1. Data preparation

Experimental data used for modelling were obtained from the response surface optimization study. A total of 20 experimental conditions were tested, and each condition was performed in triplicate, resulting in 60 data points. The input variables were fermentation time (h), fermentation temperature (°C), and inoculum level (%), while the output variables included antioxidant activity determined by DPPH, FRAP and TPC, pH value, and probiotic viability. All data were imported and processed using MATLAB (R2024b).

2.10.2. ANN construction and validation

A three-layer feedforward ANN was constructed using MATLAB Neural Network Toolbox to model the nonlinear relationships between input variables (Time, Temp, Inoculum level) and each response variable (DPPH, FRAP, TPC, pH, LAB). The network contained three input neurons, one hidden layer with 10 neurons, and one output neuron (Fig. 1). Several architectures (5, 10, 15, 20 neurons) were trained under identical settings and evaluated using Train R^2, Validation R^2 and Test R^2 (Table S1). The 10-neuron model consistently achieved high fitting accuracy and stable generalization. For instance, in DPPH prediction, it obtained Train $R^2 = 0.9861$ and Test $R^2 = 0.9742$, similar to larger models but without validation loss. Increasing neurons to 15 or 20 did not improve performance and caused overfitting, where Test R^2 notably declined, especially for FRAP, TPC and LAB (e.g., FRAP Test R^2 fell from 0.9563 at 10 neurons to 0.6670 at 20 neurons). The 5-neuron model showed lower Test R^2 and insufficient learning. Thus, the 10-neuron architecture provided the optimal balance of complexity and predictive power and was selected for subsequent optimization.

A five-fold cross-validation strategy was used to evaluate the model stability and generalization ability. Each model was trained using the Levenberg-Marquardt algorithm and evaluated through 30 repeated runs with randomized initial weights. The dataset was partitioned into training (70 %), validation (15 %), and testing (15 %) subsets. The best-performing network was selected for each output based on the highest average coefficient of determination (R^2) across the three subsets. To further evaluate the performance of model, the mean square error (MSE) and root mean square error (RMSE) were calculated. These metrics provided a quantitative measure of prediction accuracy, ensuring the reliability of the ANN models for subsequent optimization. R2, MSE, and RMSE were calculated according to Eqs. (3–5), respectively.

$$R^2 = \frac{\Sigma_{i=1}^{n} (y_i - \hat{y}_i)^2}{\Sigma_{i=1}^{n} (y_i - \bar{y})^2} \quad (3)$$

$$MSE = \frac{1}{n} \sum_{i=1}^{n} (y_i - \hat{y}_i)^2 \quad (4)$$

$$RMSE = \sqrt{\frac{1}{n} \sum_{i=1}^{n} (y_i - \hat{y}_i)^2} \quad (5)$$

Where y_i was the actual value for sample, $\hat{y}_i$ was the predicted value for the sample, $\bar{y}$ was the average value of actual values, and n was the number of samples.

2.10.3. Multi-objective optimization and TOPSIS selection

NSGA-II was implemented through the *gamultiobj* function to maximize DPPH, FRAP, TPC, and LAB, with pH constrained near 4.5 because LAB-fermented plant-based milk is commonly fermented to pH 4.5 as an endpoint before cooling and storage (Piazentin et al., 2020). The population size and maximum generation were set to 100 and 200, respectively, to provide sufficient search diversity and convergence stability, and *gaplotpareto* was enabled to monitor the evolution of the Pareto front in real time. A Pareto-optimal solution set was obtained, and only formulations with LAB $\geq$ 7 log CFU/mL were retained to ensure probiotic viability. The retained Pareto solutions were subsequently ranked using the Technique for Order Preference by Similarity to the Ideal Solution (TOPSIS), in which all responses were assigned equal weights. The final condition was selected as the compromise solution with the highest relative closeness to the ideal response profile.

2.11. Data analysis

Data analysis and response surface modeling were performed using Minitab 16.0 (Minitab Inc., USA), while the graphical representation of the response surfaces was carried out using Origin 2025 (OriginLab, Northampton, MA, USA). Artificial neural network (ANN) modeling was developed using MATLAB R2024b (MathWorks Inc., Natick, MA, USA). Optimization procedures based on and a multi-objective non-dominated sorting genetic algorithm II (NSGA-II) were implemented using MATLAB Optimization Toolbox. The compromise optimal solution was selected using the TOPSIS (Technique for Order Preference by Similarity to Ideal Solution) method. All analyses were performed in triplicate.

Table 1
Experimental range and levels of independent variables.

Independent variables	Symbol	Axial (-α)	Level (−1)	Level (0)	Level (+1)	Axial (+α)
Fermentation Time (h)	X_1	2.64	4	6	8	9.37
Fermentation Temperature (°C)	X_2	32	34	37	40	42
Starter Inoculum (%, v/v)	X_3	0.3	1	2	3	3.7

3. Results and discussion

3.1. CCD-RSM modeling

Table 2 summarizes the experimental results and model-predicted values obtained from 20 fermentation trials involving chickpea-based milk substrates. The experiments were designed to evaluate the influence of three independent variables: fermentation time (X_1: 4–8 h), fermentation temperature (X_2: 34–40 °C), and inoculum level (X_3: 1–3 % v/v) on five response parameters. The influence of linear, quadratic, and interaction components on each response variable was assessed based on the coded regression coefficients of the independent factors, as detailed in Table 3. The fitted quadratic polynomial models exhibited strong statistical significance, with all models achieving high coefficients of determination ($R^2 > 0.96$), adjusted R^2 values ranging from 0.9287 to 0.9726, and predicted R^2 values between 0.7604 and 0.9192. These

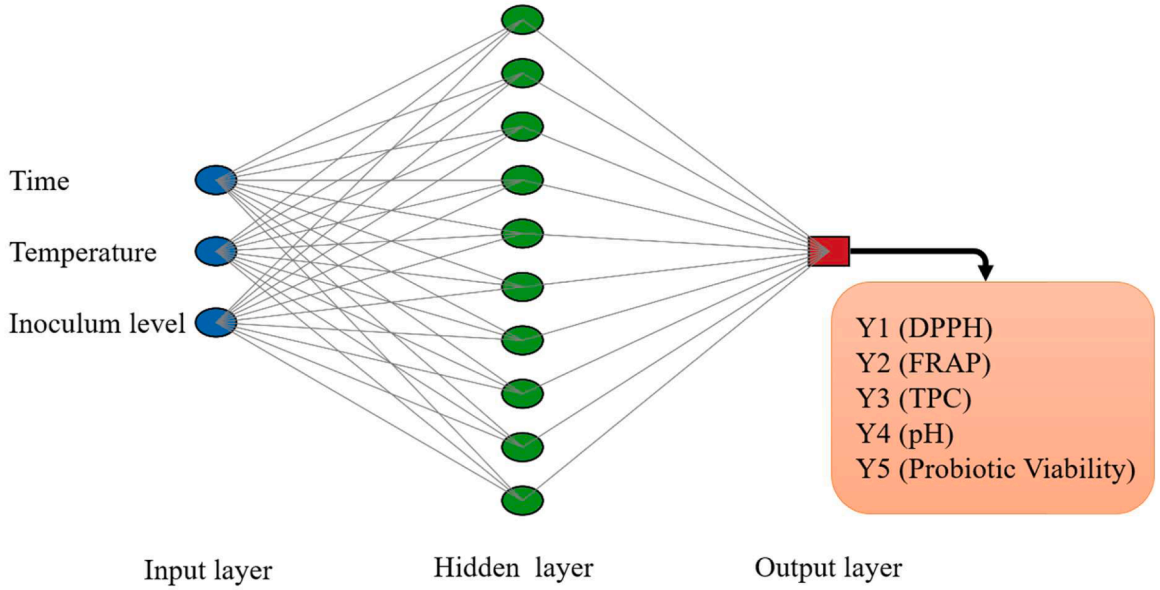

Fig. 1. Schematic representation of the neural network architecture, with output nodes illustrated in the lower right section.

metrics demonstrate the reliability and robustness of the models in capturing the response behavior under different fermentation conditions. The lack-of-fit values ($p > 0.05$ for all responses) confirmed that the fitted models were adequate with no significant deviation from the experimental data, validating their suitability for optimization. The optimal chickpea milk fermentation conditions were determined using response surface plots (Fig. 2) and optimization analysis. The ideal conditions for enhanced antioxidant activity, probiotic viability, and target pH were 6.10 h, 35.1 °C, and a starter inoculum of 2.53 %.

3.1.1. *Effect of fermentation conditions on DPPH scavenging activity*

The influence of fermentation variables on DPPH radical scavenging activity (Y_1) was modeled using a second-order polynomial regression, with model parameters presented in Table 3. The regression model showed high statistical significance ($p < 0.001$) and excellent goodness-of-fit, as reflected by the R^2 value of 0.9799, adjusted R^2 of 0.9618, and predicted R^2 of 0.8600. The lack of fit was insignificant ($p = 0.079$), confirming model adequacy.

According to the regression coefficients, all three linear terms (X_1, X_2, X_3) significantly influenced DPPH activity ($p < 0.001$). Specifically, both fermentation time (X_1) and temperature (X_2) had significant adverse linear effects, indicating that longer durations and higher temperatures reduced antioxidant capacity. This trend may be attributed to the thermal or enzymatic degradation of antioxidant compounds or metabolic consumption by probiotic strains. In contrast, starter inoculum (X_3) exhibited a significant positive effect ($p < 0.001$), suggesting that higher inoculum levels promote greater production or preservation of antioxidant metabolites, possibly via more active microbial metabolism.

The significant quadratic terms (X_1^2, X_2^2, X_3^2) further revealed the nonlinear nature of the response. The negative coefficients of X_1^2 (-1.1951), X_2^2 (-0.8839), and X_3^2 (-0.4208) imply that excessively high levels of these variables result in a decline in DPPH activity, reinforcing the notion of optimal fermentation conditions.

Interaction effects were also evident. The interaction between fermentation time and temperature ($X_1 \times X_2$) exhibited a highly significant positive effect (1.085, $p < 0.001$), suggesting a compensatory mechanism wherein the adverse effects of prolonged time could be mitigated by moderating the temperature and vice versa. Moreover, the interaction between X_1 and X_3 ($p < 0.01$) also positively contributed to DPPH retention, emphasizing the role of synergistic microbial activity under balanced time and inoculum conditions.

The response surface plots in Fig. 2A–C visually supported these statistical findings. The surface shows a saddle shape, with an apparent decline in DPPH values at high fermentation times and temperatures, confirming the adverse impact of excessive thermal and temporal stress. Fig. 2(B) illustrates a rising ridge toward higher inoculum levels, affirming its positive contribution to antioxidant preservation. Similarly, Fig. 2(C) reveals a subtle but positive elevation in DPPH activity with increasing inoculum, especially at moderate temperatures.

3.1.2. *Effect of fermentation conditions on FRAP*

The response surface model for ferric reducing antioxidant power (FRAP, Y_2) exhibited a high level of significance, with $R^2 = 0.9760$, adjusted $R^2 = 0.9543$, and predicted $R^2 = 0.8619$, alongside a non-significant lack-of-fit ($p = 0.184$). The model sufficiently captured the behavior of FRAP under varied fermentation conditions.

Fermentation time (X_1) significantly increased FRAP (0.01672, $p < 0.001$), indicating that extended fermentation enhanced reductive capacity. This may be due to microbial release or conversion of antioxidant precursors into redox-active compounds. Interestingly, this positive trend contrasts with DPPH behavior, where prolonged fermentation time negatively affected scavenging ability, suggesting distinct pathways or compound sensitivities between the two antioxidant mechanisms.

In contrast, fermentation temperature (X_2) demonstrated a substantial adverse effect (-0.05089, $p < 0.001$), implying that elevated temperatures diminish ferric-reducing power. This aligns with the thermal degradation trend observed for DPPH, reinforcing the importance of controlled thermal input for antioxidant retention.

Starter inoculum (X_3) exerted a positive but non-significant linear influence (0.00484, $p > 0.05$), suggesting a limited role in FRAP enhancement under the tested range. This differs from its pronounced positive impact on DPPH, possibly reflecting divergent microbial contributions to electron-donating versus radical-scavenging activities.

Quadratic effects further defined the curvature of FRAP responses. X_1^2 (0.01206, $p < 0.01$) had a significant positive coefficient, suggesting a progressive increase in FRAP beyond linear effects, while X_3^2 (-0.00738, $p < 0.05$) revealed a subtle diminishing return at higher inoculum levels. Notably, the temperature quadratic term (X_2^2) was not statistically significant, indicating a more linear thermal response.

Among interaction terms, the $X_1 \times X_2$ interaction was significant and

Table 2
Experimental and RSM Predicted Values of Y1-Y5 from CCD.

X_1	X_2	X_3	Y_1		Y_2		Y_3		Y_4		Y_5	
			Experimental	RSM Predicted	Experimental	RSM Predicted	Experimental	RSM Predicted	Experimental	RSM Predicted	Experimental	RSM Predicted
6.00	32	2	10.807	10.99	0.304	0.318	38.962	38.673	4.99	4.88	5.18	5.79
4.00	34	1	12.401	11.875	0.25	0.242	34.676	34.359	5.07	5.18	4.2	3.94
4.00	34	3	11.974	12.146	0.254	0.242	45.343	45.283	4.77	4.87	4.71	4.35
8.00	34	3	9.952	9.79	0.328	0.32	42.01	42.327	4.05	4.07	8.32	8.18
8.00	34	1	7.845	7.939	0.308	0.305	30.39	30.398	4.8	4.82	8.5	8.1
9.36	37	2	7.988	7.927	0.278	0.278	37.438	37.49	4	4.04	8.76	8.83
6.00	37	2	11.775	12.127	0.214	0.216	49.152	47.838	4.45	4.53	8.02	7.87
6.00	37	2	12.373	12.127	0.202	0.216	48.01	47.838	4.46	4.53	7.5	7.87
6.00	37	3.7	11.917	11.754	0.192	0.203	44.105	44.226	4.3	4.24	8.17	8.18
6.00	37	2	12.259	12.127	0.227	0.216	47.343	47.838	4.58	4.53	8.1	7.87
6.00	37	2	12.003	12.127	0.22	0.216	47.914	47.838	4.61	4.53	7.82	7.87
2.64	37	2	9.297	9.568	0.21	0.222	41.819	42.705	5.44	5.27	2.9	3.06
6.00	37	2	12.174	12.127	0.216	0.216	47.248	47.838	4.54	4.53	7.8	7.87
6.00	37	2	12.231	12.127	0.217	0.216	47.533	47.838	4.51	4.53	7.99	7.87
6.00	37	0.3	9.753	10.121	0.186	0.187	33.533	34.338	4.74	4.67	6.28	6.49
4.00	40	1	8.158	8.175	0.176	0.175	44.2	43.222	4.68	4.75	4.36	4.34
4.00	40	3	8.5	8.266	0.185	0.18	43.724	43.052	4.9	4.97	6.03	6.27
8.00	40	3	8.87	10.25	0.183	0.183	41.152	40.81	3.9	3.88	8.87	8.97
8.00	40	1	8.899	8.579	0.16	0.164	40.581	39.976	4.1	4.09	7.18	7.38
6.00	42	2	8.244	8.265	0.15	0.147	43.629	44.851	4.37	4.35	7.19	6.8

Notes: X_1, X_2, and X_3 represent fermentation time (h), temperature (°C), and inoculum level (%), respectively. Y_1, Y_2, Y_3, Y_4, and Y_5 denote DPPH (μg L-ascorbic acid/mL), FRAP (mM Fe^{2+}/L), TPC (μg GAE/mL), pH, and probiotic viability (log_{10} CFU/mL), respectively. Experimental values are the observed results obtained under the CCD design conditions, and RSM predicted values are those estimated by the fitted response surface models.

negative (−0.01875, $p < 0.01$), suggesting that the FRAP enhancing effect of prolonged fermentation was compromised when paired with elevated temperature. This interaction aligns with the DPPH activity's observed trade-off, reinforcing the antioxidant components' thermal sensitivity. Other interaction terms, including $X_1 \times X_3$ and $X_2 \times X_3$, did not reach statistical significance.

The trends are reflected in the response surface plots. The Fig. 2(D) plot shows a declining plane with increasing temperature despite time-mediated elevation in FRAP at lower thermal conditions. The surface of Fig. 2(E) reveals a pronounced curvature, confirming the quadratic relationship and minor contribution of the inoculum. In Fig. 2(F), FRAP steadily declines with rising temperature, with little modulation by inoculum level.

These results suggest that maximal FRAP activity can be achieved through prolonged fermentation at relatively low temperatures. Further supporting this observation, Yan *et al.* document that fermentation by different lactic acid bacteria (LAB) generally increases FRAP values in beverages. However, they also indicate that high temperatures can negatively impact fermentation efficacy, suggesting that elevated thermal conditions may hinder enzymatic processes necessary for promoting antioxidant compounds (Yan et al., 2023). Similarly, Nguyen et al. (2024) point out that biological compounds are susceptible to degradation when exposed to prolonged high temperatures, which can reduce antioxidant activity (Duy et al., 2020). Compared with DPPH, the positive effect of time is more prominent for FRAP, while temperature exerts a consistently adverse impact across both indices. Controlling thermal input is the most critical factor for preserving and enhancing ferric reducing capacity during chickpea milk fermentation.

3.1.3. *Effect of fermentation conditions on TPC*

The total phenolic content (TPC, Y_3) exhibited a robust fit to the second-order polynomial model, as evidenced by a high R^2 of 0.9856, an adjusted R^2 of 0.9726, and a predicted R^2 of 0.9192. The non-significant lack-of-fit ($p = 0.217$) further validated the adequacy of the model for predictive applications.

Among the linear terms, fermentation temperature (X_2) and starter inoculum level (X_3) were the dominant positive contributors to TPC, with coefficients of 1.837 and 2.940, respectively ($p < 0.001$). These findings suggest that moderate thermal input enhances phenolic release, likely through improved cell wall disruption or enzymatic activity (Zhang et al., 2025), while increased inoculum provides a higher metabolic load to facilitate microbial hydrolysis or transformation of bound phenolics. This effect may also be associated with enhanced microbial β-glucosidase activity, which may hydrolyze chickpea isoflavone glycosides, particularly conjugated precursors of biochanin A and formononetin, as well as some genistein-related phenolics, thereby increasing the proportion of extractable aglycone-type compounds (Gao et al., 2015). In contrast, fermentation time (X_1) demonstrated a significantly adverse effect (−1.551, $p < 0.001$), implying a net decline in TPC with prolonged fermentation. This reduction could be attributed to either the oxidative degradation of released phenolics or microbial assimilation over time.

All three quadratic terms (X_1^2, X_2^2, X_3^2) were significantly negative ($p < 0.001$ or $p < 0.01$), indicating nonlinear, saturation-like behavior. In particular, X_3^2 exhibited the strongest curvature (−3.025), suggesting that excessive inoculum levels may hinder phenolic accumulation, potentially due to rapid acidification or microbial overconsumption.

Among interaction terms, $X_2 \times X_3$ displayed a significant adverse effect (−2.774, $p < 0.001$), highlighting that the beneficial effect of either high temperature or inoculum is not additive. The negative $X_2 \times X_3$ interaction suggests that a moderate increase in temperature may improve matrix softening and facilitate the release of bound phenolics, while a higher inoculum level may enhance microbial enzymatic activity and accelerate the liberation of phenolic compounds. However, when both factors were elevated simultaneously, fermentation likely became excessively intensive. Higher temperature can accelerate LAB growth

Table 3
Significant coefficients ($p < 0.05$) and ANOVA results of the response surface model.

Term	Y_1	Y_2	Y_3	Y_4	Y_5
Constant	12.127***	0.2157***	47.838***	4.5287***	7.8650***
X_1	−0.4879***	0.01672***	−1.551***	−0.3655***	1.7153***
X_2	−0.8100***	−0.0509***	1.8370***	−0.1576***	0.2995*
X_3	0.4854***	0.0048	2.9400***	−0.1296**	0.5029***
X_1 X_1	−1.1951***	0.0121**	−2.7370***	0.0450	−0.6804***
X_2 X_2	−0.8839***	0.0061	−2.1480***	0.0309	−0.5549***
X_3 X_3	−0.4208**	−0.0074*	−3.0250***	−0.0257	−0.1872
X_1 X_2	1.0850***	−0.0188**	0.1790	−0.0737	−0.2810
X_1 X_3	0.3950**	0.0038	0.2510	−0.1087*	−0.0840
X_2 X_3	−0.0450	0.0010	−2.7740***	0.1388**	0.3790*
P_{lof}	0.079	0.184	0.217	0.071	0.059
R^2	0.9799	0.9760	0.9856	0.9625	0.9774
Adj R^2	0.9618	0.9543	0.9726	0.9287	0.9570
Pred R^2	0.8600	0.8619	0.9192	0.7604	0.8511

Notes: X_1, X_2, and X_3 represent fermentation time, temperature, and inoculum level, respectively. Y_1, Y_2, Y_3, Y_4, and Y_5 denote DPPH, FRAP, TPC, pH, and probiotic viability, respectively. X_1X_1, X_2X_2, and X_3X_3 represent quadratic terms, while X_1X_2, X_1X_3, and X_2X_3 represent interaction terms. P_{lof} indicates the p-value for lack-of-fit. R^2, Adj R^2, and Pred R^2 represent the coefficient of determination, adjusted coefficient of determination, and predicted coefficient of determination, respectively.
*, **, and *** indicate significance at $p < 0.05$, $p < 0.01$, and $p < 0.001$, respectively.

and acidification, and a larger inoculum can further shorten the lag phase and intensify metabolic turnover. Under these conditions, phenolics released at the early stage may not be retained efficiently, but instead may be further transformed, destabilized, or metabolically consumed (Gaur and Gänzle, 2023). Therefore, the combined elevation of temperature and inoculum level suppressed net phenolic retention, even though each factor alone was beneficial within a moderate range. Other interaction terms, including $X_1 \times X_2$ and $X_1 \times X_3$, were not statistically significant.

The surface plots provide visual confirmation of these effects. Fig. 2 (G) reveals a dome-shaped surface, with the highest TPC occurring at moderate time and temperature values. At extreme time or temperature values, phenolic content decreased markedly. In Fig. 2(H), TPC increased steadily with higher inoculum up to a point beyond which the curve flattened or declined, reinforcing the quadratic behavior. Fig. 2(I) displayed a distinct saddle shape, reflecting the negative synergy between thermal intensity and microbial density.

Compared to antioxidant capacity indicators, the TPC response shared some parallels with DPPH, particularly the detrimental effect of prolonged fermentation time. However, in contrast to DPPH and FRAP, where temperature generally exerted suppressive effects, TPC benefited from moderate temperature increases, underscoring the temperature-dependent release of phenolic compounds. Meanwhile, the impact of inoculum on TPC was more pronounced than on FRAP, aligning more closely with the DPPH trend.

3.1.4. Effect of fermentation conditions on pH

The pH value of fermented chickpea milk was significantly influenced by all three fermentation variables, as reflected by the high predictive performance of the response surface model ($R^2 = 0.9625$, Adj-$R^2 = 0.9287$, Pred-$R^2 = 0.7604$). The lack-of-fit was non-significant ($p = 0.071$), indicating that the model adequately captured the acidification behavior under varying processing conditions.

Fermentation time (X_1) exhibited the most pronounced effect on pH reduction, as evidenced by its strongly negative linear coefficient (-0.3655, $p < 0.001$). This trend corresponds to the continuous production and accumulation of organic acids, particularly lactic acid, over time. Similarly, fermentation temperature (X_2) and inoculum level (X_3) also contributed significantly to the decrease in pH (-0.1576, $p < 0.001$ and -0.1296, $p < 0.01$, respectively). The increase in microbial load and thermal energy likely promoted metabolic activity and sugar catabolism, thereby accelerating acidogenesis.

In contrast to the curvature observed in antioxidant indices, none of the quadratic terms (X_1^2, X_2^2, X_3^2) reached statistical significance, indicating a predominantly linear trend in acidification throughout the tested range. However, the significant negative interaction between fermentation time and inoculum level ($X_1 \times X_3$, -0.1087, $p < 0.05$) revealed that increased inoculum amplified the acidifying effect of prolonged fermentation. Conversely, the interaction between temperature and inoculum ($X_2 \times X_3$, 0.1388, $p < 0.01$) displayed a counterbalancing effect, suggesting that at higher inoculum levels, the elevated temperature did not linearly intensify acid production, potentially due to inhibition of lactic acid bacteria growth by excessive fermentation temperature. These observations are well aligned with the response surface plots. Fig. 2(J) demonstrates a sharp decline in pH with increasing fermentation time and temperature. In Fig. 2(K), pH decreased rapidly at higher inoculum levels, especially at extended fermentation times. Fig. 2(L) illustrates a more moderate curvature, confirming the buffering effect between thermal and microbial contributions.

3.1.5. Effect of fermentation conditions on probiotic viability

The proliferation of *Lactiplantibacillus plantarum* PC4 during chickpea milk fermentation strongly depended on the dynamic interplay among time, temperature, and inoculum level. Unlike antioxidant or pH responses, which were predominantly unidirectional or nonlinear, probiotic viability followed a typical microbial growth trajectory characterized by an initial expansion phase and saturation or inhibition at higher parameter levels.

Fermentation time emerged as the primary driving factor. As shown in Fig. 2(M) and (N), cell counts increased steeply during early fermentation, with a tendency to stabilize beyond 6–7 h. This trend corresponds with the exponential growth phase of lactic acid bacteria, during which nutrients are abundant and environmental stress is minimal. However, excessive prolongation led to a slight decline, likely due to acidification (as supported by pH trends) and depletion of essential growth factors (Webber et al., 2014).

Inoculum level exerted a dual effect: moderate increases (up to 2.5 %) promoted viable counts through accelerated colonization and metabolic synergy. In contrast, further increases yielded diminishing returns, as observed in the curvature of the X_3^2 term. This plateau may reflect overcrowding, pH drop, or quorum sensing–mediated growth regulation.

Temperature showed a relatively mild yet consistent effect, with cell viability rising gradually from 34 °C to 38 °C. However, in high inoculum concentrations, the interaction between temperature and starter level ($X_2 \times X_3$) became more pronounced, yielding a noticeable uplift in probiotic survival.

Comparing this behavior to antioxidant responses, notable divergences emerge. While DPPH and TPC peaked and then declined

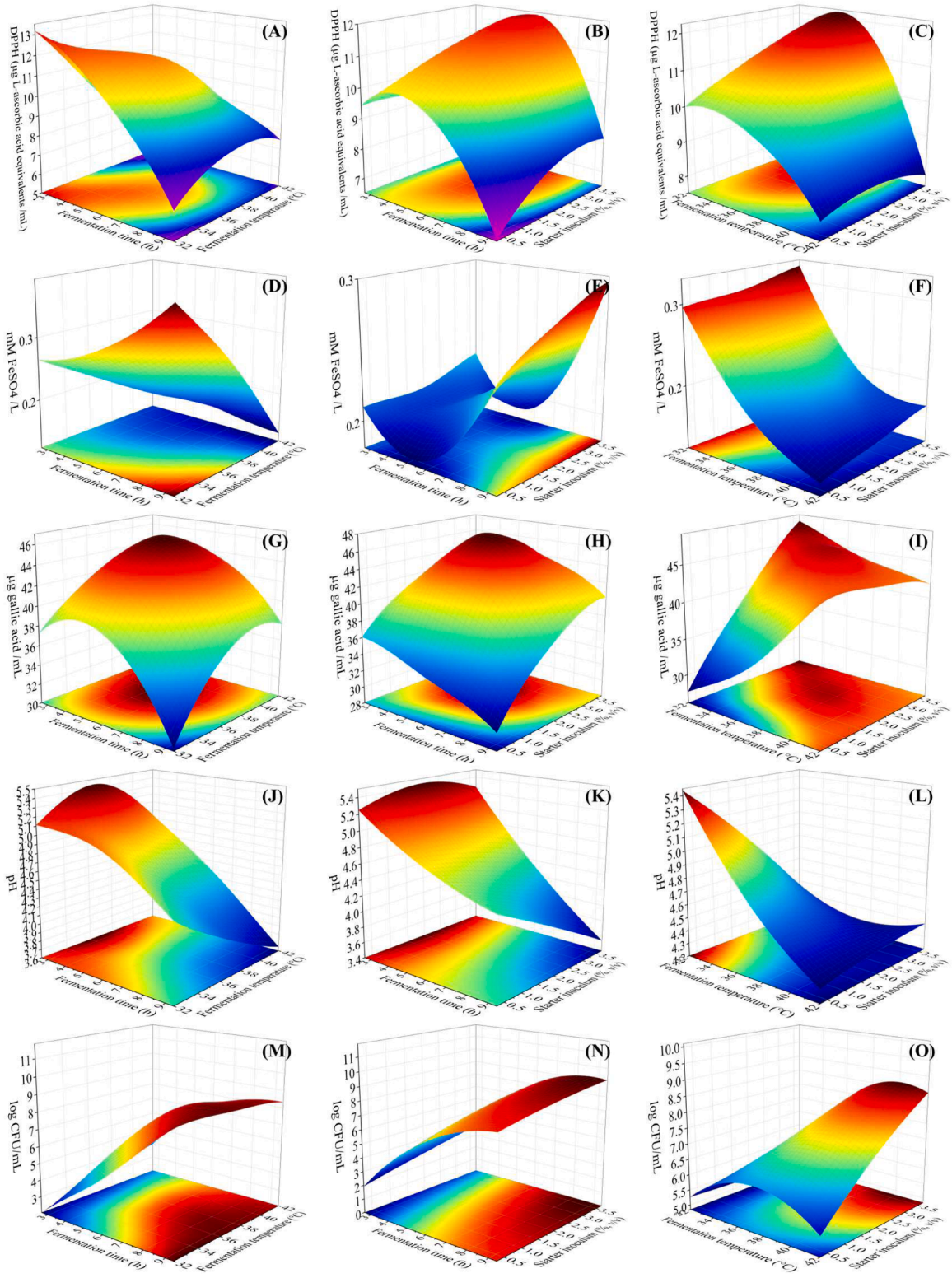

Fig. 2. Response surface plots depicting the interactive effects of fermentation time, temperature, and inoculum level on the antioxidant capacity (DPPH: A–C; FRAP: D F), total phenolic content (TPC: G–I), pH (J–L), and probiotic viability (M–O) in chickpea milk fermented by Lactiplantibacillus plantarum PC4.

under higher fermentation stress, probiotic viability remained stable or continued rising under similar conditions. This distinction highlights microbial proliferation's resilience relative to plant phenolics' oxidative stability. Conversely, the inverse association with pH confirms that active acidification was tightly linked to viable cell biomass, reinforcing the view that LAB growth and acid metabolism proceed in parallel.

3.1.6. *Multi-factor interaction analysis*

The interaction effects among fermentation time, temperature, and inoculum level revealed non-additive influences on fermentation outcomes. For antioxidant indices, $X_1 \times X_2$ and $X_2 \times X_3$ interactions alternated between synergistic and antagonistic effects, depending on the response considered. Acidification showed a synergistic acceleration under

prolonged time and high inoculum, while probiotic viability benefited from $X_2 \times X_3$ interactions at moderate temperatures. These findings, together with the response surface plots (Fig. 2), indicate that the balance between factors is more decisive than any single variable, underscoring the importance of multi-factor interactions in optimizing chickpea milk fermentation.

3.2. ANN modeling

3.2.1. ANN model performance based on 5-fold cross-validation

The ANN models showed stable learning and generalization across all five folds (Table 4). For DPPH, Train R^2 ranged from 0.9701 to 0.9906, and Test R^2 remained consistently high between 0.9532 and 0.9832, demonstrating that the network did not overfit and was able to reliably predict antioxidant scavenging activity under unseen conditions. FRAP also showed strong overall performance, although fold 2 exhibited a lower Test R^2 (0.8161) compared to the other folds (0.9260–0.9763). This fluctuation indicates moderate sensitivity of reducing power to sample variability or measurement noise, yet the remaining folds maintained high prediction accuracy.

The TPC model produced stable results across folds, with Test R^2 between 0.8939 and 0.9576. Slightly lower performance in fold 2 suggests that total polyphenol content may display greater biological variability across fermentation batches, but all folds still achieved acceptable prediction accuracy above 0.89, confirming that ANN effectively captured polyphenol release dynamics.

For pH, Test R^2 ranged from 0.8907 to 0.9503. Although slightly lower than antioxidant indicators, the narrow range implies stable prediction of acidification behavior. Since pH changes gradually and are primarily driven by lactic acid accumulation, even a Test R^2 around 0.90 is suitable for practical monitoring and process prediction.

LAB showed the highest stability and predictive strength. Train R^2 and validation R^2 were consistently above 0.99, while Test R^2 remained between 0.9847 and 0.9961 for all folds. These results confirm that microbial growth patterns are highly learnable from fermentation time, temperature and inoculum level, and the model captures the underlying nonlinear relationships with minimal overfitting.

The five-fold results demonstrate that ANN models generalize well across all functional and microbiological responses. The small differences between Train and Test R^2 indicate that the networks did not rely excessively on training data, and the consistently high Test R^2 values highlight strong robustness against sample variation.

Table 4
5-fold cross-validation performance of ANN models (denormalized test data).

Response	Fold	Train R^2	Validation R^2	Test R^2
DPPH	1	0.9798	0.9896	0.9730
	2	0.9701	0.9502	0.9832
	3	0.9796	0.9802	0.9718
	4	0.9906	0.9711	0.9532
	5	0.9891	0.9796	0.9745
FRAP	1	0.9581	0.9886	0.9672
	2	0.7820	0.9774	0.8161
	3	0.9705	0.9827	0.9260
	4	0.9772	0.9424	0.9763
	5	0.9380	0.9691	0.9495
TPC	1	0.9725	0.9699	0.9162
	2	0.9775	0.8858	0.8939
	3	0.9670	0.9697	0.9292
	4	0.9533	0.9826	0.9516
	5	0.9593	0.9869	0.9576
pH	1	0.9608	0.9813	0.9126
	2	0.9841	0.9324	0.8907
	3	0.9674	0.9088	0.9503
	4	0.9217	0.9736	0.9179
	5	0.9688	0.9011	0.9056
LAB	1	0.9916	0.9990	0.9888
	2	0.9960	0.9969	0.9847
	3	0.9956	0.9937	0.9923
	4	0.9920	0.9988	0.9961
	5	0.9961	0.9737	0.9934

Notes: R^2 values were calculated based on denormalized data. Train R^2, Validation R^2, and Test R^2 represent the coefficients of determination for the training, validation, and test subsets, respectively, in each fold of the 5-fold cross-validation procedure. DPPH, 2,2-diphenyl-1-picrylhydrazyl radical scavenging activity; FRAP, ferric reducing antioxidant power; TPC, total phenolic content; LAB, lactic acid bacteria viability.

3.2.2. Validation of MSE trends during ANN training

Fig. 3A-E presents the training performance plots of the ANN models for DPPH, FRAP, TPC, pH, and LAB, respectively. The mean squared error (MSE) values shown correspond to the validation dataset at each epoch.

In the DPPH model (Fig. 3A), the validation MSE decreased rapidly during the first three epochs and stabilized thereafter, reaching a minimum value of 0.01919 at epoch 5. The FRAP model (Fig. 3B) exhibited a steep decline in validation MSE within the first epoch, reaching 0.00225.

For the TPC model (Fig. 3C), the validation MSE gradually decreased across the first 6 epochs and reached a minimum value of 0.002633 at epoch 7. The pH model (Fig. 3D) showed a progressive reduction in validation MSE up to epoch 6, achieving a minimum value of 0.001495. The LAB model (Fig. 3E) exhibited a sharp decrease in validation MSE during the initial 3 epochs, attaining a minimum value of 0.000339 at epoch 4.

Throughout the training process, no sudden increases in validation MSE were observed for any of the models, and the validation curves remained generally stable after reaching their respective minimum.

3.2.3. Regression analysis of ANN model fitting

The predictive performance of the ANN model was evaluated by comparing experimental and predicted values of DPPH, FRAP, TPC, pH, and LAB in the training, validation, and test subsets (Fig. 4). All response variables showed a close overlap between true and predicted curves, indicating that the network successfully captured the nonlinear relationships within the fermentation system.

For antioxidant indicators, the prediction of DPPH demonstrated excellent fitting, with R^2 values of 0.9865 in training, 0.9836 in validation, and 0.9830 in testing. FRAP also showed strong accuracy, with R^2 reaching 0.9742, 0.9930, and 0.9471 in the three subsets. These values confirm that the ANN model effectively learned the chemical responsiveness of fermented chickpea milk, where antioxidant capacity is affected by phenolic release, microbial metabolism, and fermentation duration. TPC prediction remained reliable, with R^2 values of 0.9699, 0.9723, and 0.9050. The slightly lower R^2 in the test set can be attributed to higher experimental variation in phenolic content, which is sensitive to both fermentation intensity and spray drying conditions. The predictions of pH also achieved high accuracy, with R^2 values of 0.9780, 0.9820, and 0.9511, reflecting the stable model recognition of acidification dynamics associated with organic acid synthesis.

The most accurate prediction was obtained for LAB viability. R^2 reached 0.9936 in training, 0.9969 in validation, and 0.9963 in testing, demonstrating that microbial growth followed highly learnable kinetic patterns. The close alignment of experimental and predicted LAB values indicates strong generalization ability and confirms that the ANN does not overfit the data.

3.3. Pareto front generation and compromise solution selection

Based on the Pareto front distributions in Fig. 5 and the ranked solutions presented in Table 5, the highest TOPSIS score (0.643) was associated with a fermentation time of 7.40 h, a temperature of 35.95 °C, and an inoculum level of 2.22 %. Under these conditions, the ANN model predicted DPPH of 11.15 μg L-ascorbic acid /mL, FRAP of 0.297 μmol Fe^{2+}/mL, TPC of 44.42 mg GAE/mL, pH of 4.14, and LAB viability of 8.81 $\log_{10}$ CFU/mL. All responses were assigned equal weights during

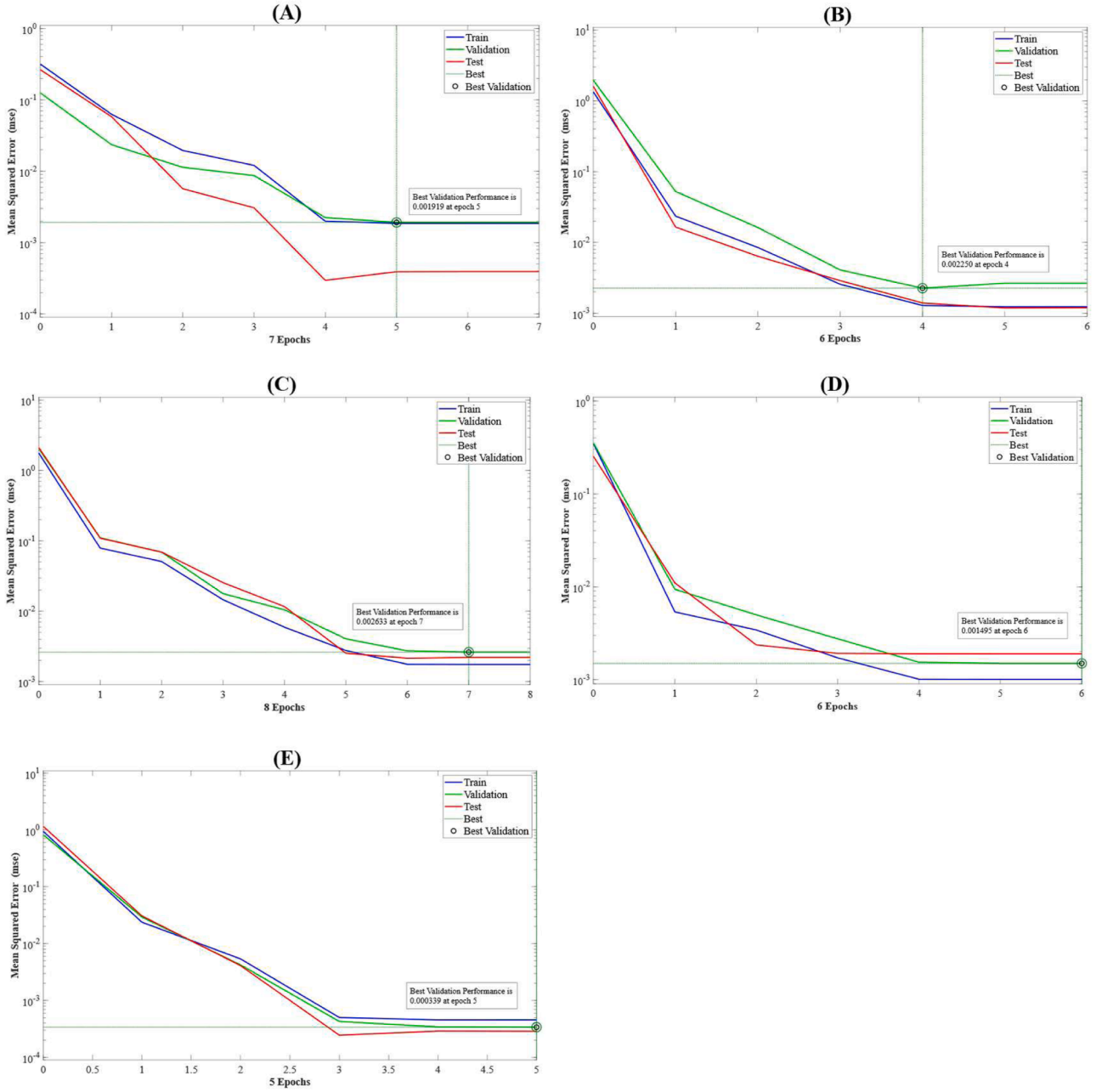

Fig. 3. Training performance curves for each ANN model: (A) DPPH, (B) FRAP, (C) TPC, (D) pH, and (E) LAB. Mean squared error (MSE) trends are plotted for training, validation, and test datasets across epochs.

TOPSIS ranking. This solution occupied a central position on the Pareto surface and demonstrated a balanced response profile, simultaneously achieving high antioxidant capacity, acceptable acidity, and satisfactory probiotic survival.

The second-ranked solution (TOPSIS 0.643) required a shorter fermentation period (6.17 h) at 36.52 °C and resulted in higher DPPH and TPC values. However, LAB viability decreased to 7.83 log CFU/mL, reducing the overall composite performance. The remaining Pareto-optimal solutions exhibited comparable trade-offs, as formulations with enhanced antioxidant activity frequently presented lower LAB counts or pH values deviating from the desirable fermentation range. Therefore, the selected condition was considered the most appropriate because it provided a more favorable overall combination of responses among the retained Pareto solutions, rather than the highest value for any single indicator. These findings indicate that the optimal point is not defined by any single biochemical parameter, but by the convergence of antioxidant responses, microbial stability, and acidity into an integrated compromise. As an evolutionary, population-based method, NSGA-II effectively maintained solution diversity through crowding distance sorting, enabling comprehensive exploration of the multi-dimensional design space (Lee et al., 2007). Integrating ANN surrogate models enhanced computational efficiency, offering a practical and robust approach for optimizing functional food formulations.

3.5. Validation and verification of the predictive model

Table 6 compares the predicted values generated by the two optimization strategies with their corresponding experimental measurements. Overall, ANN—NSGA-II exhibited higher predictive accuracy than RSM-CCD for most response variables. For DPPH, the ANN prediction deviated from the experimental mean by only 1.61 %, compared with 3.00 % for RSM. A similar trend was observed for FRAP and TPC,

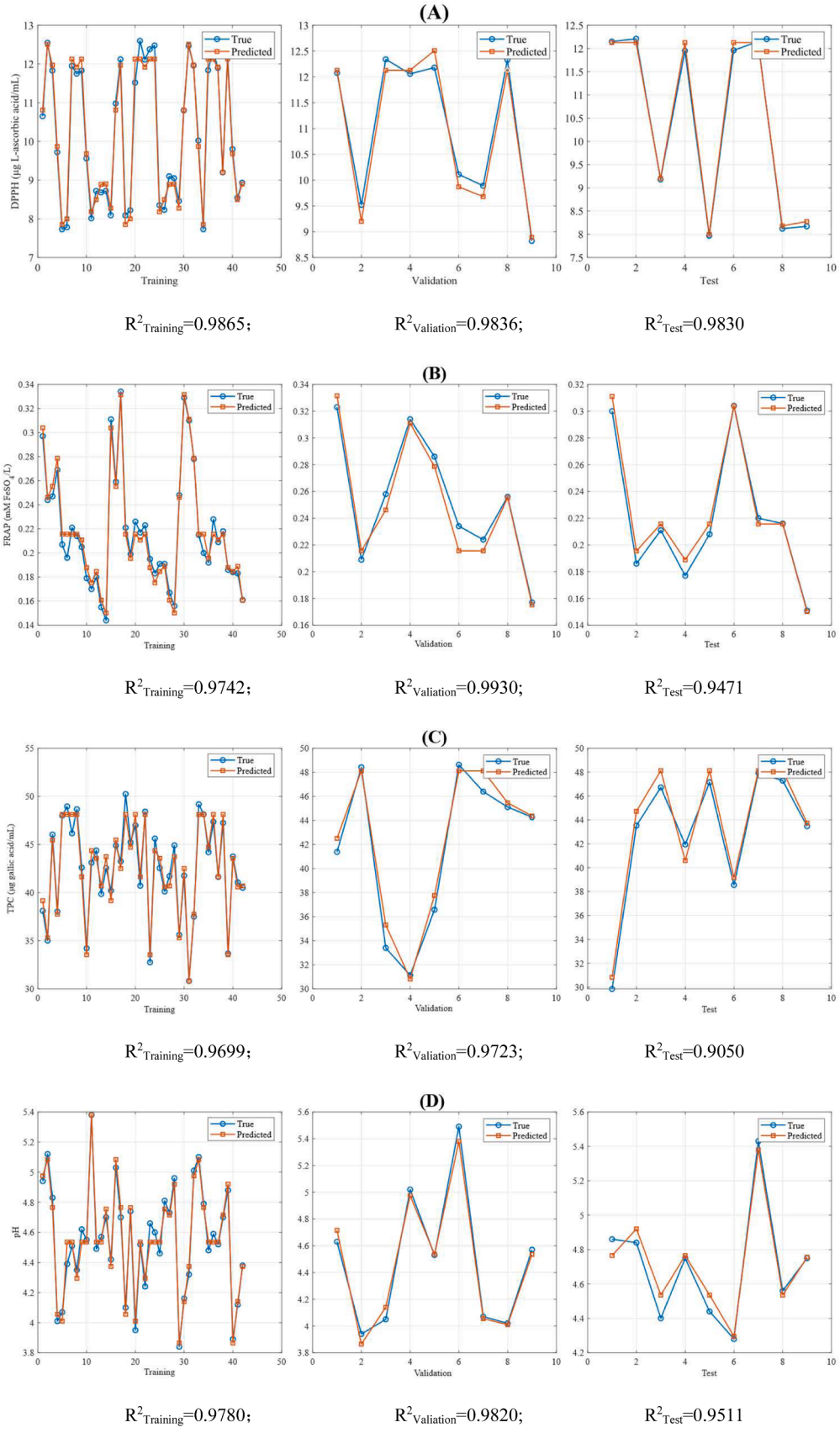

Fig. 4. Comparison between true and ANN predicted values for (A) DPPH, (B) 17 FRAP, (C) TPC, (D) pH, and (E) LAB across training, validation, and test sets.

where RSM produced relatively large errors of 9.92 % and 8.66 %, while the ANN model yielded substantially smaller deviations of 1.35 % and

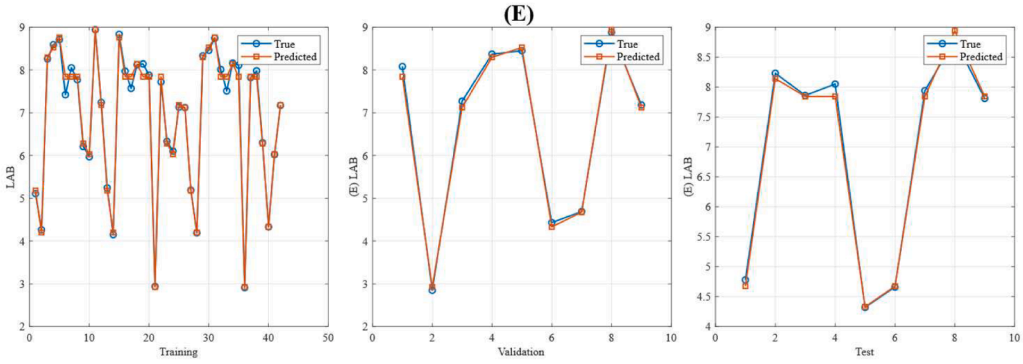

$R^2_{Training}$=0.9936; $R^2_{Valiation}$=0.9969; R^2_{Test}=0.9963

Fig. 4. (*continued*).

0.32 %, respectively. These results indicate that the traditional second-order polynomial model was less effective in capturing the complex response surface associated with antioxidant formation, whereas the neural network more effectively learned the nonlinear relationships among fermentation variables. This interpretation was further supported by the one-sample *t*-test results, in which the predicted and experimental values for DPPH, FRAP, and TPC under both optimization strategies were not significantly different ($p > 0.05$), despite the clearly smaller numerical deviations obtained by ANN—NSGA-II.

Both models showed relatively small deviations for pH, which is consistent with the gradual acidification behavior of lactic fermentation. In this case, RSM showed slightly better agreement with the experimental value, with an error of 3.78 %, whereas ANN gave a somewhat larger deviation of 4.64 %. However, the *t*-test indicated that the differences between predicted and experimental pH values were statistically significant for both models ($p < 0.05$), suggesting that even though the absolute errors were limited, neither model fully captured the acidification endpoint with sufficient precision. This result may reflect the high sensitivity of pH to subtle biochemical changes during the late stage of fermentation. Therefore, compared with the antioxidant-related responses, pH appeared to be more difficult to predict accurately using either modeling approach.

In the case of probiotic viability, ANN again demonstrated higher accuracy, with a 4.03 % error compared with 5.34 % for RSM, confirming its stronger capability in representing microbial growth behavior. Nevertheless, the one-sample *t*-test showed that the differences between predicted and experimental viable counts were statistically significant for both models ($p < 0.01$). This finding suggests that, although ANN—NSGA-II provided a closer numerical approximation than RSM-CCD, both models still had limited precision in estimating the final viable cell concentration. Compared with pH, however, ANN achieved a smaller relative error and therefore retained a practical advantage for viability prediction.

The experimental validation demonstrates that ANN—NSGA-II achieved a more reliable description of the multi-response fermentation system than RSM-CCD. The consistently lower prediction errors for antioxidant activity, total phenolic release, and viable cell counts suggest that the ANN model better accommodated the inherent nonlinearity and biological variability of the process. More importantly, when numerical deviation and statistical comparison were considered together, ANN—NSGA-II showed clear superiority over RSM-CCD for the major functional responses, especially DPPH, FRAP, TPC, and probiotic viability. Although its pH prediction was slightly less accurate than that of RSM, the overall performance of ANN—NSGA-II remained superior across the most important quality attributes. These findings highlight the advantage of ANN-based multi-objective optimization for data-driven design and control of plant-based fermentation products. Although direct machine learning-guided optimization studies in fermented plant-based milks remain limited, related work in adjacent fermentation systems supports the value of the present framework. ANN has been reported to better accommodate nonlinear input-output relationships than conventional empirical models, particularly when multiple process variables act simultaneously. In mixed-sugar fermentation, multi-input and multi-output ANN models improved predictive accuracy and generalization, indicating their suitability for biologically coupled systems (Huang et al., 2023). In fermented blueberry juice, regression modeling combined with a genetic algorithm improved phenolic enrichment and volatile quality, although the optimization still relied on polynomial fitting rather than ANN-based surrogate modeling (Liao et al., 2023). ANN has also shown stronger predictive performance than SVM in other fermentation processes involving multivariable nonlinear responses (Silva et al., 2022). These studies collectively indicate that machine learning-assisted optimization has potential in complex fermentation systems.

3.6. Evaluation of β-glucosidase activity

The evaluation of β-glucosidase activity in chickpea milk showed significant differences among unfermented, 6.10 h, and 7.40 h fermentation groups (Fig. 6). The unfermented sample exhibited negligible activity (0.0008 U/mL), suggesting that chickpea milk contained only minimal endogenous β-glucosidase. After 6.10 h of fermentation, the activity increased to 0.041 U/mL, indicating that microbial metabolism contributed to enzyme production and activation. At 7.40 h, the activity further increased to 0.053 U/mL, which was significantly higher than both the unfermented and 6.10 h groups ($p < 0.05$).

The increase in β-glucosidase activity during fermentation suggests a potential mechanistic linkage between enzymatic hydrolysis and phenolic release, as lactic acid bacteria can secrete β-glucosidases that hydrolyze glycosidic bonds and liberate aglycones from isoflavone glycosides (Rekha and Vijayalakshmi, 2011). Similar increases in β-glucosidase activity have been reported in other legume-based fermented products, where the enzyme plays a role in enhancing the bioavailability of phenolic compounds and antioxidant properties (Ping et al., 2025). The higher activity observed at 7.40 h compared with 6.10 h suggests a time-dependent increase; however, the relatively smaller increment indicates that enzyme production may approach a plateau due to nutrient limitation or product feedback inhibition.

3.7. Evaluation of organic acids

The concentrations of organic acids in fermented chickpea milk are shown in Table S3. Among the five targeted acids, only citric acid, D-tartaric acid, and L-lactic acid were detected, while L-malic acid and succinic acid were not detected in either the RSM-CCD or the ANN—NSGA-II optimized samples. Citric acid remained relatively

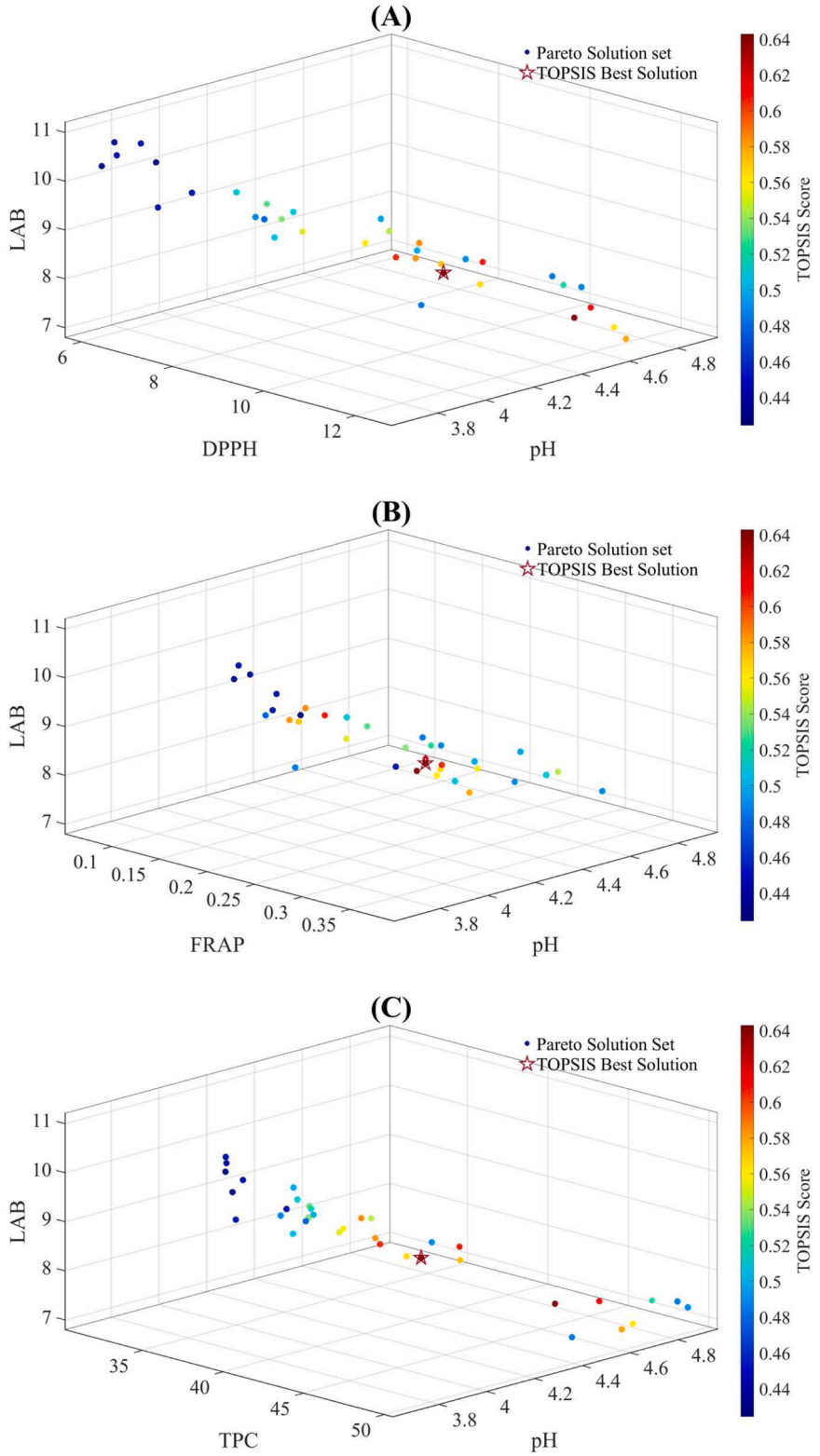

Fig. 5. 3D Pareto fronts of ANN—NSGA-II optimization results. Points are colored by TOPSIS score, and the red star indicates the TOPSIS best solution.

stable, with concentrations of 0.551 ± 0.002 mg/mL and 0.464 ± 0.002 mg/mL in the RSM-CCD and ANN—NSGA-II groups, respectively, indicating that prolonged fermentation did not increase its level. D-tartaric acid rose significantly under ANN—NSGA-II optimization (0.831 ± 0.009 vs 0.709 ± 0.002 mg/mL, $p < 0.05$), suggesting enhanced sourness and improved flavor complexity. The most substantial change occurred in lactic acid, which increased markedly from 1.416 ± 0.006 mg/mL under RSM-CCD to 2.453 ± 0.001 mg/mL under ANN—NSGA-II ($p < 0.05$). As the primary metabolite of lactic fermentation, its pronounced accumulation reflects intensified microbial glycolysis and directly explains the stronger pH reduction and flavor improvement achieved under optimized conditions.

Table 5
Top ten Pareto-optimal fermentation conditions selected by TOPSIS scoring from NSGA-II optimization with LAB ≥ 7 log CFU/mL.

TOPSIS Score	X_1	X_2	X_3	Y_1	Y_2	Y_3	Y_4	Y_5
0.64	7.40	35.95	2.22	11.15	0.30	44.42	4.14	8.81
0.64	6.17	36.52	2.79	12.47	0.21	48.37	4.43	7.83
0.61	5.70	37.36	2.17	12.00	0.18	48.77	4.59	7.71
0.61	5.98	38.51	3.08	11.57	0.17	45.57	4.22	9.03
0.61	7.78	35.46	2.27	10.21	0.32	42.17	4.12	8.92
0.59	6.74	37.81	3.49	11.42	0.21	42.97	3.98	9.69
0.58	7.45	37.92	2.98	11.66	0.21	44.75	3.92	9.52
0.58	5.48	36.74	2.25	12.25	0.21	48.70	4.69	7.00
0.57	5.97	39.13	2.78	10.85	0.15	46.14	4.18	8.85
0.57	6.80	36.59	1.27	10.57	0.25	39.64	4.40	8.08

Notes: X_1, X_2, and X_3 represent fermentation time (h), temperature (°C), and inoculum level (%), respectively. Y_1, Y_2, Y_3, Y_4, and Y_5 denote DPPH (μg L-ascorbic acid/mL), FRAP (mM Fe^{2+}/L), TPC (μg GAE/mL), pH, and probiotic viability (log_{10} CFU/mL), respectively. The TOPSIS score was used to rank the Pareto-optimal solutions obtained from NSGA-II optimization, with higher values indicating better overall performance. Only solutions satisfying the constraint of LAB ≥ 7 log CFU/mL were included.

3.8. Evaluation of volatile compounds

Volatile profiles of chickpea milk before and after fermentation were characterized by SPME–GC/MS, revealing diverse aroma-active compounds across multiple chemical classes (Supplementary Table S4). Fig. 7A summarizes the changes in total concentrations of the main categories. Acids increased markedly during fermentation, rising from 37.78 μg/kg at 0 h to 202.13 μg/kg at 7.40 h. This shift reflects enhanced microbial activity, particularly the production of acetic, hexanoic, and octanoic acids, which introduced sour and complex notes. Alcohols also accumulated, from 593.10 μg/kg at 0 h to 920.61 μg/kg at 6.10 h, followed by a slight decline. Long-chain alcohols such as 1-hexanol, 1-heptanol, and 1-nonanol showed consistent increases. In contrast, unsaturated alcohols including (E)-2-octen-1-ol declined, suggesting microbial transformation or degradation. Several new alcohols, such as tetrahydromyrcenol and (E)-2-nonen-1-ol, appeared only under ANN—NSGA-II optimized conditions, indicating broader metabolic activation compared with RSM-CCD.

Aldehydes were the predominant class in unfermented samples, with a total concentration of 814.20 μg/kg. Fermentation reduced aldehyde levels to 623.78 μg/kg at 6.10 h and 507.19 μg/kg at 7.40 h. Hexanal, the major aldehyde, decreased from 473.10 μg/kg to 79.82 μg/kg. Because hexanal has a very low odor threshold, its reduction is closely linked to the attenuation of beany and oxidized notes (Harper et al., 2022). Nonanal, dodecanal, and (E)-2-octenal also decreased significantly, supporting the role of microbial conversion of aldehydes into less odorous derivatives (Tangyu et al., 2023).. Notably, (E,E)-2,4-decadienal, associated with fried and fatty aroma, increased under ANN—NSGA-II optimization, suggesting selective formation of certain aldehydes despite the overall decline.

The alkene fraction declined drastically, from 236.50 μg/kg at 0 h to 6.96 μg/kg at 7.40 h. Compounds such as 2,4-dimethyl-1-heptene and 1-dodecene disappeared after fermentation. The reduction of these unstable hydrocarbons reduced waxy or solvent-like notes. Esters, absent in the unfermented samples, were generated after fermentation. The detection of vinyl hexanoate indicates esterification between accumulating acids and alcohols, contributing to fruity and sweet notes. Ketones and furans showed minor variations, although 2-pentyl furan persisted across all conditions.

The multivariate analysis in Fig. 7B confirms these compositional changes. Principal component analysis separated the three fermentation stages clearly, with PC1 (55.6 %) and PC2 (35.9 %) explaining most of the variance. ANN—NSGA-II optimized samples showed the greatest divergence from the unfermented baseline, reflecting deeper modification of the volatile matrix. This separation consists of higher levels of alcohols, acids, and esters and lower aldehyde and alkene contents.

3.9. Sensory analysis

The sensory evaluation of chickpea milk samples is presented in Fig. 8. The radar chart (Fig. 8A) shows distinct differences between unfermented and fermented samples. Unfermented chickpea milk received higher scores in color uniformity and beany flavor, while its fermented aroma and acidity were rated very low. In contrast, both fermented samples showed a clear rise in fermented aroma and acidity, especially at 7.40 h, consistent with the higher levels of organic acids and fermentation volatiles reported in Section 3.6. Thickness and smoothness were comparable across samples, although the unfermented

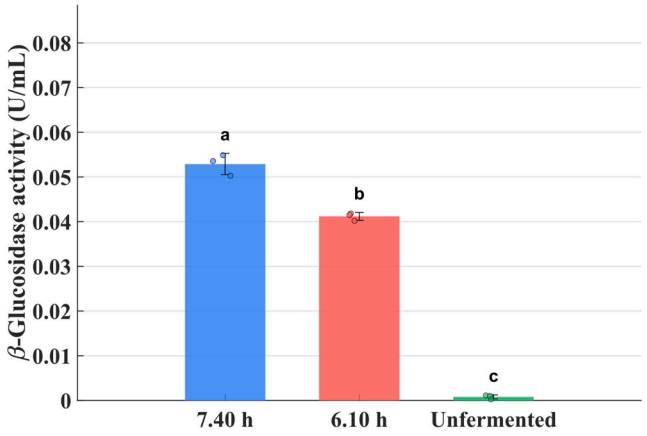

Fig. 6. Comparison of β-glucosidase activity in chickpea milk: unfermented, 6.10 h, and 7.40 h fermentation.
Note: Different letters (a–c) above the bars indicate significant differences among groups ($p < 0.05$) according to one-way ANOVA followed by Tukey test.

Table 6
Experimental validation of RSM-CCD and ANN—NSGA-II optimized fermentation conditions for functional chickpea milk.

Response Variables	Goal	RSM-CCD			ANN—NSGA-II		
		Predicted	Experimental ($n = 3$)	Error	Predicted	Experimental ($n = 3$)	Error
DPPH (μg L-ascorbic acid /mL)	Maximize	12.389	12.017±0.516ns	3.00 %	11.149	11.328 ± 0.287 ^{ns}	1.61 %
FRAP (mM Fe^{2+} /L)	Maximize	0.252	0.227±0.015ns	9.92 %	0.297	0.293 ± 0.013 ^{ns}	1.35 %
TPC (μg GAE /mL)	Maximize	47.377	43.273±3.145ns	8.66 %	44.421	44.563 ± 1.835 ^{ns}	0.32 %
pH	Target=4.50	4.50	4.67±0.058*	3.78 %	4.138	4.33 ± 0.058*	4.64 %
Probiotic viability (log CFU/ml)	Maximize	7.637	8.045±0.041**	5.34 %	8.810	8.455 ± 0.027**	4.03 %

Note: All the values are means ± standard deviation from triplicate determinations. Error (%) was calculated as the absolute percentage deviation between the predicted and experimental values: Error (%) = |(Experimental − Predicted)/Predicted| × 100. For pH, the target value was set at 4.50. Superscripts indicate the significance of the difference between predicted and experimental values based on a one-sample *t*-test: ns, not significant ($p > 0.05$);.
* $p < 0.05$;.
** $p < 0.01$.

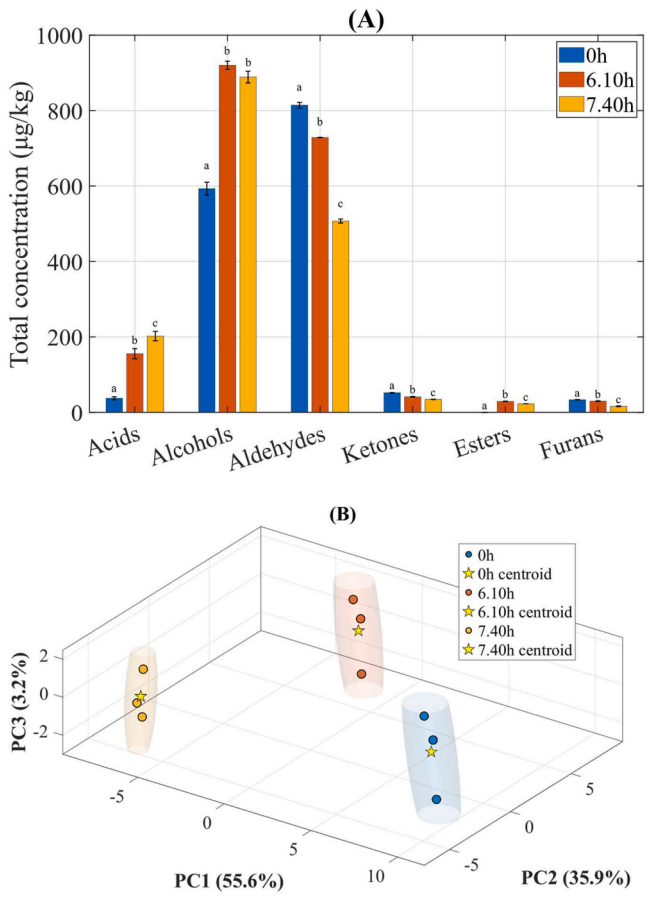

Fig. 7. (A) Total concentrations of different volatile compound classes (μg/kg) in chickpea milk at 0 h, 6.10 h, and 7.40 h of fermentation. Error bars represent standard deviations (n = 3). Different letters above bars indicate significant differences (p < 0.05). (B) 3D PCA score plot of GC–MS data, showing the distribution of volatile profiles across unfermented (0 h) and fermented samples (6.10 h and 7.40 h). Each dot represents a replicate, stars indicate group centroids, and shaded ellipsoids represent the 95 % confidence regions of each group.

milk tended to be slightly smoother. Aftertaste intensity was elevated in fermented samples, likely due to the combined perception of acidity and aroma compounds. Notably, color uniformity remained one of the discriminating visual attributes, even though fermentation did not cause a dramatic change in the overall color tone. In plant-based milk systems, visual uniformity is closely associated with appearance quality and colloidal stability, because fermentation may alter particle dispersion, aggregation behavior, or phase separation. Therefore, a lower score for color uniformity in fermented chickpea milk may reflect slight changes in physical homogeneity rather than a substantial shift in color itself.

The PCA biplot (Fig. 8B) further illustrates the distribution of samples in relation to the sensory attributes. PC1 (52.3 % of variance) mainly differentiated fermented from unfermented milk. Fermented aroma and acidity loaded on the positive side of PC1 and were associated with both fermented samples. . In contrast, color uniformity and beany flavor aligned with the negative side of PC1 and were associated with the unfermented sample. This distribution confirms that fermentation shifted the sensory profile from beany-dominant to acid- and aroma-dominant attributes. PC2 (16.2 % of variance) was less discriminative, but smoothness and aftertaste contributed to subtle differences between 6.10 h and 7.40 h samples.

These observations are consistent with the volatile compound results discussed in Section 3.6. The decline in aldehydes such as hexanal corresponded with reduced beany flavor, while the increase in acids and esters supported the enhanced perception of fermented aroma and acidity. These data suggest that fermentation not only modifies chemical composition but also leads to perceptible improvements in sensory quality. A limitation of this sensory analysis is the relatively small trained panel (n = 14). Although this may constrain the generalizability of the results, the structured training procedure and the agreement with compositional data indicate that the main sensory trends were captured reliably.

4. Conclusions

This study confirmed that chickpea milk provides a suitable environment for fermentation by *Lactiplantibacillus plantarum* PC4, resulting in improved biochemical, microbiological, and sensory quality. Fermentation enhanced antioxidant activity and total phenolic release, increased β-glucosidase activity, and generated organic acids that lowered pH to a desirable range. Volatile profiling further showed a substantial decline in aldehydes responsible for beany notes, together with the formation of alcohols, acids, and esters that contributed to a cleaner fermented aroma. The modelling approach revealed that fermentation performance was governed by nonlinear interactions among time, temperature, and inoculum level; neural networks captured these patterns more accurately than polynomial regression. Multi-objective optimization successfully identified a balanced condition that simultaneously supported high antioxidant responses, strong probiotic viability, and acceptable acidity, and validation experiments closely matched model predictions. These findings establish a data-driven foundation for developing chickpea-based probiotic beverages with improved flavor and nutritional properties.

From an industrial perspective, the ANN—NSGA-II framework may also provide a useful basis for fermentation scale-up, particularly in processes where multiple quality attributes change nonlinearly and require coordinated monitoring and control. With further integration of online sensors and real-time process data, this approach may support more adaptive process management in industrial fermentation. However, this study was conducted under laboratory-scale batch conditions using a limited set of process variables. Further validation under pilot-scale or industrial conditions will be needed before broader application.

Funding

The authors gratefully acknowledge the financial support from Universiti Putra Malaysia under the research grant Geran Universiti Putra Malaysia (GP/2023/9753300). The study was carried out under the Universiti Research Development Program (URDP) — Functional Food Development & Future Food research group.

Ethics statement

The sensory evaluation involving human participants was reviewed and approved by the Ethics Committee for Research Involving Human Subjects, Universiti Putra Malaysia (JKEUPM) (Approval No. JKEUPM-2025-284; approval date: 24 May 2025). All procedures were conducted in accordance with relevant institutional guidelines. Participants' privacy rights were respected, and informed consent was obtained from all participants prior to participation.

CRediT authorship contribution statement

Ping Tang: Writing – review & editing, Writing – original draft, Visualization, Methodology, Formal analysis, Data curation. **Siew-Young Quek:** Supervision, Conceptualization. **Yi-Chen Lo:** Supervision, Conceptualization. **Somayeh Gholivand:** Writing – review & editing. **Ming-Yang Cui:** Writing – review & editing. **Aliah Zannierah Mohsin:** Supervision, Conceptualization. **Nurul Hanisah Juhari:** Supervision, Conceptualization. **Anis Shobirin Meor Hussin:** Supervision,

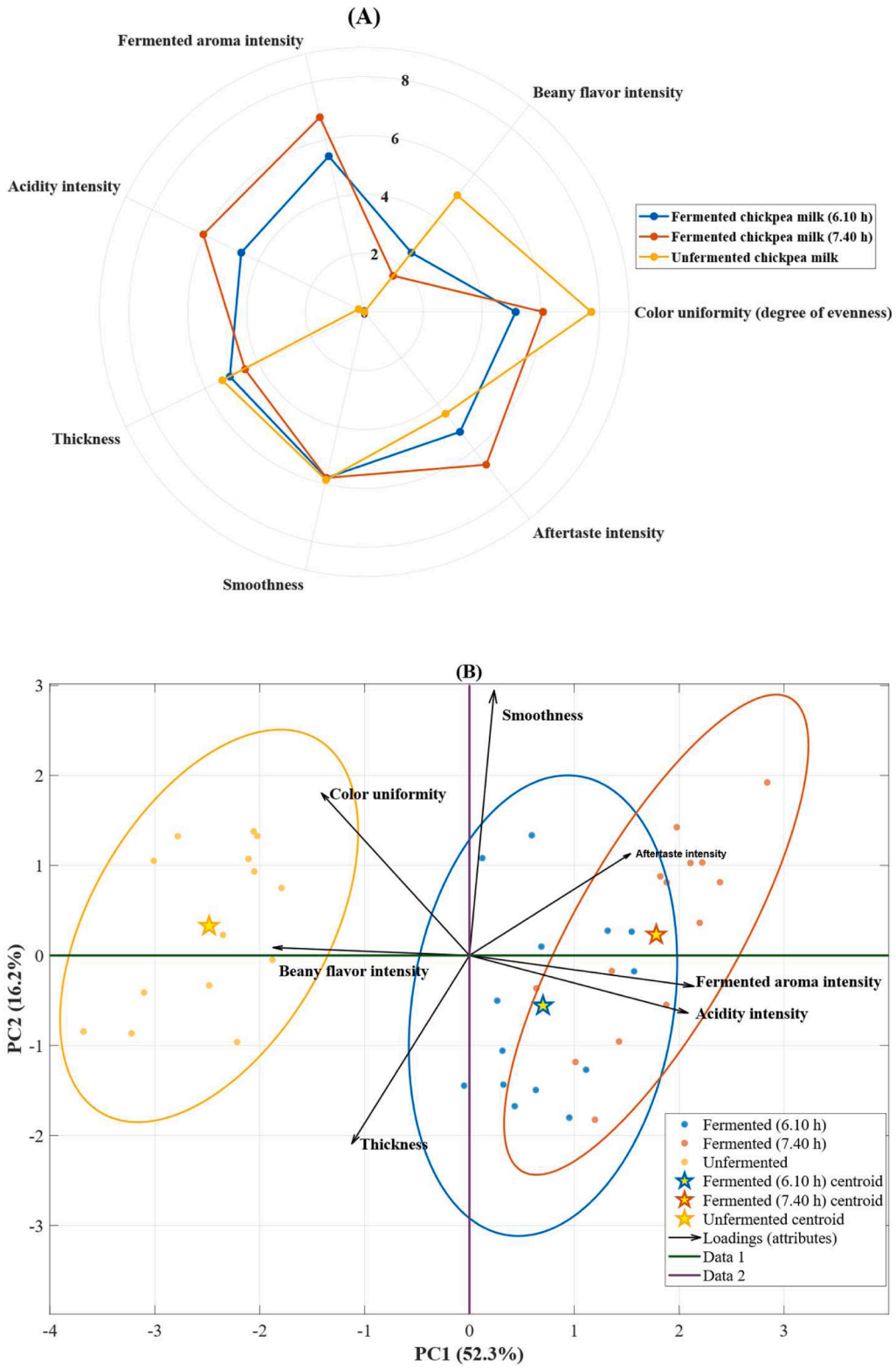

Fig. 8. Sensory profile and principal component analysis (PCA) of chickpea milk samples.
(A) Radar plot of sensory attributes, including color uniformity, beany flavor, fermented aroma, acidity, thickness, smoothness, and aftertaste intensity. (B) PCA scores plot of individual panelists with 95 % confidence ellipses and attribute loadings. Different colors represent unfermented chickpea milk and fermented chickpea milk at 6.10 h and 7.40 h, respectively.

Conceptualization.

Declaration of competing interest

The authors declare that they have no competing financial interests or personal relationships that could have influenced the work presented

in this paper.

Acknowledgements

The authors gratefully acknowledge the support and generosity of Universiti Putra Malaysia

Supplementary materials

Supplementary material associated with this article can be found, in the online version, at doi:10.1016/j.fufo.2026.101032.

Data availability

Data will be made available on request.

References

Abadl, M.M.T., Marzlan, A.A., Sulaiman, R., Abas, F., Meor Hussin, A.S., 2023. Optimization of coconut milk Kefir beverage by RSM and screening of its metabolites and peptides. Fermentation 9, 430. 10.3390/fermentation9050430.

Abbaspour, N., 2024. Fermentation's pivotal role in shaping the future of plant-based foods: an integrative review of fermentation processes and their impact on sensory and health benefits. Appl. Food Res. 4, 100468. 10.1016/j.afres.2024.100468.

Anzian, A., Hussin, M., Qadir, R., Azhari, S.H., Juhari, N.H., Yusof, Y.A., Adnan, H., Meor Hussin, A.S., 2024. Exploring the physicochemical and microbiological properties of glutinous rice (Tapai pulut) fermented using Lactobacillus plantarum: a comprehensive characterization using 1H NMR. Food Biosci. 62, 105165. 10.1016/j.fbio.2024.105165.

Benzie, I.F.F., Strain, J.J., 1999. [2]Ferric reducing/antioxidant power assay: direct measure of total antioxidant activity of biological fluids and modified version for simultaneous measurement of total antioxidant power and ascorbic acid concentration. pp. 15–27. 10.1016/S0076-6879(99)99005-5.

Bhagya Raj, G.V.S., Dash, K.K., 2022. Comprehensive study on applications of artificial neural network in food process modeling. Crit. Rev. Food Sci. Nutr. 62, 2756–2783. 10.1080/10408398.2020.1858398.

Chaturvedi, S., Chakraborty, S., 2021. Review on potential non-dairy synbiotic beverages: a preliminary approach using legumes. Int. J. Food Sci. Technol. 56, 2068–2077. 10.1111/ijfs.14779.

Chen, J., Wang, Q., Wu, Yuting, Wu, Yue, Sun, Y., Ding, Y., Wei, Z., Manickam, S., Pan, S., Yang, J., Tao, Y., 2023. Ultrasound-assisted fermentation of ginkgo kernel juice by lactiplantibacillus plantarum: microbial response and juice composition development. Ultrason. Sonochem. 99, 106587. 10.1016/j.ultsonch.2023.106587.

De Farias Silva, C.E., Costa, G.Y.S.C.M., Ferro, J.V., de Oliveira Carvalho, F., da Gama, B. M.V., Meili, L., dos Santos Silva, M.C., Almeida, R.M.R.G., Tonholo, J., 2022. Application of machine learning to predict the yield of alginate lyase solid-state fermentation by Cunninghamella echinulata: artificial neural networks and support vector machine. React. Kinet., Mech. Catal. 135, 3155–3171. 10.1007/s11144-022-02293-9.

De Villa, R., Roasa, J., Mine, Y., Tsao, R., 2023. Impact of solid-state fermentation on factors and mechanisms influencing the bioactive compounds of grains and processing by-products. Crit. Rev. Food Sci. Nutr. 63, 5388–5413. 10.1080/10408398.2021.2018989.

Duy, N.Q., Nguyen, T.M.H., Lam, T.D., Pham, T.N., Thanh, T.T., 2020. Extraction and determination of antioxidant activity of Vietnamese butterfly pea (<i>Clitoria ternatia</i> L.). Mater. Sci. Forum 977, 207–211. 10.4028/www.scientific.net/MSF.977.207.

Gao, Y., Yao, Y., Zhu, Y., Ren, G., 2015. Isoflavone content and composition in chickpea (*Cicer arietinum* L.) sprouts germinated under different conditions. J. Agric. Food Chem. 63, 2701–2707. 10.1021/jf5057524.

Gaur, G., Gänzle, M.G., 2023. Conversion of (poly)phenolic compounds in food fermentations by lactic acid bacteria: novel insights into metabolic pathways and functional metabolites. Curr. Res. Food Sci. 6, 100448. 10.1016/j.crfs.2023.100448.

Harper, A.R., Dobson, R.C.J., Morris, V.K., Moggré, G., 2022. Fermentation of plant-based dairy alternatives by lactic acid bacteria. Microb. Biotechnol. 15, 1404–1421. 10.1111/1751-7915.14008.

Huang, X.Y., Ao, T.J., Zhang, X., Li, K., Zhao, X.Q., Champreda, V., Runguphan, W., Sakdaronnarong, C., Liu, C.G., Bai, F.W., 2023. Developing high-dimensional machine learning models to improve generalization ability and overcome data insufficiency for mixed sugar fermentation simulation. Bioresour. Technol. 385. 10.1016/j.biortech.2023.129375.

Jayasree Joshi, T., SV, S., Mohan, L., Nandagopal, P., Arakal, J.J., 2024. Functional metabolites of probiotic lactic acid bacteria in fermented dairy products. Food Humanit. 3, 100341. 10.1016/j.foohum.2024.100341.

Lee, F.C., Rangaiah, G.P., Ray, A.K., 2007. Multi-objective optimization of an industrial penicillin V bioreactor train using non-dominated sorting genetic algorithm. Biotechnol. Bioeng. 98, 586–598. 10.1002/bit.21443.

Liao, W., Shen, J., Manickam, S., Li, S., Tao, Y., Li, D., Liu, D., Han, Y., 2023. Investigation of blueberry juice fermentation by mixed probiotic strains: regression modeling, machine learning optimization and comparison with fermentation by single strain in the phenolic and volatile profiles. Food Chem. 405. 10.1016/j.foodchem.2022.134982.

Lopes, M., Pierrepont, C., Duarte, C.M., Filipe, A., Medronho, B., Sousa, I., 2020. Legume beverages from Chickpea and Lupin, as new milk alternatives. Foods 9, 1458. 10.3390/foods9101458.

Matsuura, M., Sasaki, J., Murao, S., 1995. Studies on β -glucosidases from soybeans that hydrolyze daidzin and genistin: isolation and characterization of an isozyme. Biosci. Biotechnol. Biochem. 59, 1623–1627. 10.1271/bbb.59.1623.

Mishra, P., Mishra, S., Mahanta, C.L., 2014. Effect of maltodextrin concentration and inlet temperature during spray drying on physicochemical and antioxidant properties of amla (Emblica officinalis) juice powder. Food Bioprod. Process. 92, 252–258. 10.1016/j.fbp.2013.08.003.

Nametala, C.A.L., Souza, A.M., Pereira Júnior, B.R., da Silva, E.J., 2020. A simulator based on artificial neural networks and NSGA-II for prediction and optimization of the grinding process of superalloys with high performance grinding wheels. CIRP J. Manuf. Sci. Technol. 30, 157–173. 10.1016/j.cirpj.2020.05.004.

Nguyen, C.T., Nguyen Di, K., Phan, H.C., Kha, T.C., Nguyen, H.C., 2024. Microencapsulation of noni fruit extract using gum arabic and maltodextrin – Optimization, stability and efficiency. Int. J. Biol. Macromol. 269, 132217. 10.1016/j.ijbiomac.2024.132217.

Okoro, O.V., Hippolyte, D.E.C., Nie, L., Karimi, K., Denayer, J.F.M., Shavandi, A., 2025. Machine learning-based predictive modeling and optimization: artificial neural network-genetic algorithm vs. response surface methodology for black soldier fly (Hermetia illucens) farm waste fermentation. Biochem. Eng. J. 218, 109685. 10.1016/j.bej.2025.109685.

Pavani, M., Singha, P., Rajamanickam, D.T., Singh, S.K., 2024. Impact of extrusion processing on bioactive compound enriched plant-based extrudates: a comprehensive study and optimization using RSM and ANN-GA. Future Foods 9, 100286. 10.1016/j.fufo.2023.100286.

Pennells, J., Trigona, L., Patel, H., Ying, D., 2024. Ingredient functionality of soy, chickpea, and pea protein before and after dry heat pretreatment and low moisture extrusion. Foods 13. 10.3390/foods13142168.

Piazentin, A.C.M., da Silva, T.M.S., Florence-Franco, A.C., Bedani, R., Converti, A., de Souza Oliveira, R.P., 2020. Soymilk fermentation: effect of cooling protocol on cell viability during storage and in vitro gastrointestinal stress. Braz. J. Microbiol. 51, 1645–1654. 10.1007/s42770-020-00369-z.

Ping, T., Mohsin, A.Z., Juhari, N.H., Hussin, A.S.M., 2025. Comparative machine learning strategies for improving antioxidant properties and aroma quality in fermented mung bean milkby Lactobacillus plantarum PC4. Int. J. Food Microbiol. 111443. 10.1016/j.ijfoodmicro.2025.111443.

Rekha, C.R., Vijayalakshmi, G., 2011. Isoflavone phytoestrogens in soymilk fermented with β-glucosidase producing probiotic lactic acid bacteria. Int. J. Food Sci. Nutr. 62, 111–120. 10.3109/09637486.2010.513680.

Rincon, L., Braz Assunção Botelho, R., de Alencar, E.R., 2020. Development of novel plant-based milk based on chickpea and coconut. LWT 128, 109479. 10.1016/j.lwt.2020.109479.

Tangyu, M., Fritz, M., Tan, J.P., Ye, L., Bolten, C.J., Bogicevic, B., Wittmann, C., 2023. Flavour by design: food-grade lactic acid bacteria improve the volatile aroma spectrum of oat milk, sunflower seed milk, pea milk, and faba milk towards improved flavour and sensory perception. Microb. Cell Fact. 22, 133. 10.1186/s12934-023-02147-6.

Vallath, A., Shanmugam, A., 2022. Study on model plant based functional beverage emulsion (non-dairy) using ultrasound – A physicochemical and functional characterization. Ultrason. Sonochem. 88, 106070. 10.1016/j.ultsonch.2022.106070.

Verma, S., Pant, M., Snasel, V., 2021. A comprehensive review on NSGA-II for multi-objective combinatorial optimization problems. IEEE Access 9, 57757–57791. 10.1109/ACCESS.2021.3070634.

Wang, L., Kang, J., 2022. A review of artificial neural networks for chemical process optimization and compound property prediction. Asian J. Adv. Res. Rep. 100–108. 10.9734/ajarr/2022/v16i12453.

Wang, S., Chelikani, V., Serventi, L., 2018. Evaluation of chickpea as alternative to soy in plant-based beverages, fresh and fermented. LWT 97, 570–572. 10.1016/j.lwt.2018.07.067.

Webber, D.M., Hettiarachchy, N.S., Li, R., Horax, R., Theivendran, S., 2014. Phenolic profile and antioxidant activity of extracts prepared from fermented heat-stabilized defatted rice bran. J. Food Sci. 79. 10.1111/1750-3841.12658.

Yan, X.-T., Zhang, Z., Wang, Y., Zhang, W., Zhang, L., Liu, Y., Chen, D., Wang, W., Ma, W., Qian, J.-Y., Gu, R., 2023. Antioxidant capacity, flavor and physicochemical properties of FH06 functional beverage fermented by lactic acid bacteria: a promising method to improve antioxidant activity and flavor of plant functional beverage. Appl. Biol. Chem. 66, 7. 10.1186/s13765-022-00762-2.

Yang, J., Paulino, R., Janke-Stedronsky, S., Abawi, F., 2007. Free-radical-scavenging activity and total phenols of noni (Morinda citrifolia L.) juice and powder in processing and storage. Food Chem. 102, 302–308. 10.1016/j.foodchem.2006.05.020.

Yu, T., Liu, R., Peng, C., 2016. Application of improved NSGA-II to multi-objective optimization of a coal-fired boiler combustion electronical systems in green food bases. Adv. J. Food Sci. Technol. 10, 577–582. 10.19026/ajfst.10.2187.

Zăvoianu, A.-C., Bramerdorfer, G., Lughofer, E., Silber, S., Amrhein, W., Peter Klement, E., 2013. Hybridization of multi-objective evolutionary algorithms and artificial neural networks for optimizing the performance of electrical drives. Eng. Appl. Artif. Intell. 26, 1781–1794. 10.1016/j.engappai.2013.06.002.

Zhang, P., Tang, F., Cai, W., Zhao, X., Shan, C., 2022. Evaluating the effect of lactic acid bacteria fermentation on quality, aroma, and metabolites of chickpea milk. Front. Nutr. 9. 10.3389/fnut.2022.1069714.

Zhang, P., Zhang, J., Li, L., Gu, T., Chen, S., Wang, J., Gao, M., 2025. The release of bound phenolics to enhance the antioxidant activity of cornmeal by liquid fermentation with Bacillus subtilis. Foods 14, 499. 10.3390/foods14030499.
Zhang, X., Zhang, Q., Li, Y., Zhang, H., 2023. Modeling and optimization of photo-fermentation biohydrogen production from co-substrates basing on response surface methodology and artificial neural network integrated genetic algorithm. Bioresour. Technol. 374, 128789. 10.1016/j.biortech.2023.128789.
Zheng, Z., Guo, X., Zhu, K., Peng, W., Zhou, H., 2016. The optimization of the fermentation process of wheat germ for flavonoids and two benzoquinones using EKF-ANN and NSGA-II. RSC Adv. 6, 53821–53829. 10.1039/C5RA27004A.